Magnitude, frequency and climate forcing of global volcanism during the last glacial period as seen in Greenland and Antarctic ice cores (60-9 ka)

Jiamei Lin[1], Anders Svensson[1], Christine S. Hvidberg[1], Johannes Lohmann[1], Steffen Kristiansen[1], Dorthe Dahl-Jensen[1,5], Jørgen P. Steffensen[1], Sune O. Rasmussen[1], Eliza Cook[1], Helle Astrid Kjær[1], Bo M. Vinther[1], Hubertus Fischer[2], Thomas Stocker[2], Michael Sigl[2], Matthias Bigler[2], Mirko Severi[3], Rita Traversi[3], Robert Mulvaney[4]

[1]Physics of Ice, Climate and Earth, Niels Bohr Institute, University of Copenhagen, 2100, Denmark

[2]Climate and Environmental Physics, Physics Institute & Oeschger Center for Climate Change Research, University of Bern, Sidlerstrasse 5, Bern, Switzerland

[3]Department of Chemistry, University of Florence, Florence, Italy

[4]British Antarctic Survey, Cambridge, UK

[5]Centre for Earth Observation Science, University of Manitoba, Winnipeg, Manitoba, Canada R3T 2N2

Corresponding authors: Jiamei Lin (jm.lin@nbi.ku.dk), Anders Svensson (as@nbi.ku.dk)

Abstract. Large volcanic eruptions occurring in the last glacial period can be detected by their accompanying sulfuric acid deposition in continuous ice cores. Here we employ continuous sulfate and sulfur records from three Greenland and three Antarctic ice cores to estimate the emission strength, the frequency and the climatic forcing of large volcanic eruptions that occurred during the second half of the last glacial period and the early Holocene, 60-9 ka years before AD 2000 (b2k). Over most of the investigated interval the ice cores are synchronized making it possible to distinguish large eruptions with a global sulfate distribution from eruptions detectable in one hemisphere only. Due to limited data resolution and large variability in the sulfate background signal, particularly in the Greenland glacial climate, we only list Greenland sulfate depositions larger than 20 kg km^{-2} and Antarctic sulfate depositions larger than 10 kg km^{-2}. With those restrictions, we identify 1113 volcanic eruptions in Greenland and 740 eruptions in Antarctica within the 51 ka period - where the sulfate deposition of 85 eruptions is found at both poles (bipolar eruptions). Based on the ratio of Greenland and Antarctic sulfate deposition, we estimate the latitudinal band of the bipolar eruptions and assess their approximate climatic forcing based on established methods. Twenty-five of the identified bipolar eruptions are larger than any volcanic eruption occurring in the last 2500 years and 69 eruptions are estimated to have larger sulfur emission

strengths than the Tambora, Indonesia eruption (1815 AD). Throughout the investigated period, the frequency of volcanic eruptions is rather constant and comparable to that of recent times. During the deglacial period (16-9 ka b2k), however, there is a notable increase in the frequency of volcanic events recorded in Greenland and an obvious increase in the fraction of very large eruptions. For Antarctica, the deglacial period cannot be distinguished from other periods. This confirms the suggestion that the isostatic unloading of the Northern Hemisphere (NH) ice sheets may be related to the enhanced NH volcanic activity. Our ice-core based volcanic sulfate records provide the atmospheric sulfate burden and estimates of climate forcing for further research on climate impact and understanding the mechanism of the Earth system.

1. Introduction

The dispersal of gas, aerosols and ash particles by volcanic eruptions play a major role in the climate system (Gao et al., 2007; Robock, 2000). Large volcanic eruptions injecting sulfuric gases into the stratosphere and forming sulfate aerosols have a global or hemispheric cooling effect of several degrees lasting for several years after the eruption (Sigl et al., 2015; Sinnl et al., CPD, 2021).

Estimations of volcanic stratospheric sulfur injections and of the timing and frequency of large volcanic eruptions are essential for the ability to understand and model past and future global climate conditions (Timmreck et al., 2016). For the last 1200 to 2500 years, the ice-core based volcanic forcing records derived from Greenland and Antarctica (Crowley and Unterman, 2013; Gao et al., 2008; Toohey and Sigl, 2017) provide an essential forcing record for climate model simulations (Jungclaus et al., 2017), supporting detection and attribution studies (Schurer et al., 2014) including those applied in the IPCC. However, so far the global ice-core based volcanic record of the last glacial period is poorly documented.

1.1 Ice-core records of volcanic sulfate deposition

Several studies have reconstructed the volcanic sulfate deposition for part or all of the Holocene in Greenland (Cole-Dai et al., 2009; Gao et al., 2008; Sigl et al., 2013) or in Antarctica (Kurbatov et al., 2006; Castellano et al., 2004; Plummer et al., 2012; Nardin et al., 2020; Cole-Dai et al., 2021). Sigl et al. (2015) applied accurately dated ice cores synchronized between the two hemispheres to reconstruct global volcanism over the last 2500 years. This so-called bipolar synchronization allows to distinguish large global eruptions from those of hemispheric or more regional impact. During the last 2500 years, they identified 50 global (bipolar) volcanic eruptions, 5 of which had a sulfur emission strength larger or similar to the Tambora eruption occurring in

Indonesia in 1815 CE. Prior to the last glacial maximum no bipolar volcanic sulfate deposition record is currently available from ice cores.

One conclusion drawn from historical eruptions is that there is a significant variability of the same volcanic event in the sulfate deposition records derived from different ice cores both on a regional and a local scale (Sigl et al., 2014; Gao et al., 2007). Part of this regional variability can be explained by the difference in sulfate deposition fluxes at different locations. For example, in Antarctica where geographical distances are large, the sulfate deposition at a specific site will be strongly dependent on the location of the eruption, governing wind patterns, seasonality, etc. Another reason for the lateral sulfate deposition variability is the amount and patchiness of snowfall, which may locally enhance the sulfate deposition for high snowfall areas compared to low snowfall areas for a volcanic event. Moreover, there may be more absent sulfate deposition events caused by post depositional processes on the snow surface, such as wind erosion (Gautier et al., 2016). The spatial variability of sulfate deposition in Antarctica was studied at 19 sites covering the past 2000 years by Sigl et al. (2014), and here both accumulation and post-deposition effects were found to be important factors. In particular, on the East Antarctic plateau where snow-accumulation is very low, the sulfate deposition is lower than at more coastal and higher accumulation sites in Antarctica. The snow accumulation effect is also observed in Greenland (Gao et al., 2007), although the effect is much less pronounced here, because the accumulation rates are more similar in Central Greenland than in different parts of Antarctica. In order to reduce the accumulation bias, Gao et al. (2008) selected five large low-latitude volcanic events from 54 Arctic and Antarctic ice cores and calculated the mean ratio of deposition in individual ice cores; they then applied the deposition ratio between different cores to correct the sulfate deposition for all events in all cores to obtain the Arctic and Antarctic mean sulfate depositions. In general, it is clear that more robust volcanic deposition patterns can be obtained when larger sets of ice cores are included, preferably ice cores from high-accumulation sites should be applied (Gao et al., 2007; Sigl et al., 2014).

One complication related to the derivation of volcanic sulfate deposition in ice cores is the thinning of the ice layers with increasing depth and age. Due to glacier flow, the annual layers and thus the volcano-derived sulfate deposition becomes thinned with depth; an effect that is most pronounced at high-accumulation sites and close to bedrock. In central Greenland, typical thinning rates of annual layers in the 60-10 ka range are 50-90% depending on age and local flow conditions (Johnsen et al., 2001). To calculate the sulfate deposition of a specific eruption from a measured ice concentration a correction for the thinning at the corresponding depth is needed to obtain the past annual accumulation rate. Thinning functions are obtained from ice flow modelling,

and thus, there is a site-specific dependency on accurate flow modelling associated with the sulfate deposition determination.

1.2 Studies of the frequency of volcanic eruptions

The volcanic sulfate record of the Greenland GISP2 ice core has been investigated by Zielinski et al. (1997), who found that there has been increased volcanic activity during the deglacial period (22-8 ka b2k) as compared to the average activity of the last glacial cycle. This is interpreted as being related to the tectonic isostatic response to the melting of the large ice sheets during that period. Based on the global volcanic databases (Siebert and Simkin, 2002; Bryson et al., 2006), Huybers and Langmuir (2009) found that volcanism increased two to six times during the deglacial period, 12-7 ka b2k, as compared to the average level of eruptions during 40-0 ka b2k interval.

In Antarctica, Castellano et al. (2004) determined the frequency of volcanic eruptions over the last 45 ka based on the EDC ice core. They found a rather constant level of volcanic activity throughout that period except for the most recent millennia, where the activity shows an increase. Kurbatov et al. (2006) detected volcanic signals during the last 12 ka in the Siple Dome A ice core from West Antarctica. They found that the number of volcanic sulfate signals is decreasing with age, possibly related to the relatively low sampling resolution in the deeper part of that core. Recently, Cole-Dai et al. (2021) used the high-accumulation WAIS Divide ice core to determine a fairly constant Holocene eruption frequency with larger-than-Tambora (1815 AD) events occurring approximately once per millennium. Note, however, that all these reconstructions differ in their volcanic signal detection method, which may lead to spurious trend in peak frequencies.

1.3 Volcanic events identified in ice cores with tephra and sulfate peak synchronization

In historical times, the volcanic origin of an ice-core acidity spike may be corroborated by a precise dating of the ice core (Sigl et al., 2015). Further back in time, as the uncertainty of both the ice-core dating and the dating of the volcanic eruptions increases, the origin of a volcanic ice-core layer can only be determined if it is associated with a volcanic ash (tephra) deposition in the ice (Gronvold et al., 1995). However, tephra layers are not always coinciding with sulfate peaks (Davies et al., 2010) and most volcanic sulfate signals have no tephra associated with them. The ice-core volcanic source identification is important as it helps to constrain the magnitude – interpreted here as sulfur emission strength rather than the mass of material erupted (Pyle, 2015) –

and the climate forcing of the eruption. Furthermore, it allows for a more detailed comparison to modelling studies.

In the last glacial period, many Greenland tephra deposits have been associated with Icelandic eruptions while around a dozen of identified tephra layers originate in North America and Eastern Asia (Abbott and Davies, 2012; Bourne et al., 2015; Davies et al., 2014; Cook et al., 2021 (in preparation)). In Antarctica, tephra layers have been identified and associated with eruptions occurring within Antarctica and in the Southern Hemisphere (Narcisi et al., 2005; Narcisi et al., 2010; Narcisi et al., 2012). Recently, Mcconnell et al. (2017) identified tephra from the long-lasting and halogen-rich Antarctic Mount Takahe eruption that occurred around 17.80 ka. Tephra of the Oruanui eruption from the Taupo volcano in present-day New Zealand has been identified and dated to 25.32 ka BP1950 in the West Antarctic Ice Sheet Divide ice core (WDC) (Dunbar et al., 2017).

Volcanic eruptions generally do not deposit tephra in both Greenland and Antarctica, so the bipolar synchronization of sulfur spikes in the ice cores is dependent on an alternative matching technique. Svensson et al. (2020) applied annual layer counting in both Greenland and Antarctic ice cores to match patterns of volcanic eruptions leading to the identification of some 80 bipolar eruptions in the 60-12 ka interval. For the Holocene, a bipolar synchronization of volcanic eruptions was released with the AICC2012 time scale (Veres et al., 2013). Using sulfur isotopes, it has recently become possible to test if sulfate has indeed reached the stratosphere, which is a prerequisite for being globally distributed, as the sulfate undergoes characteristic isotope fractionation in the stratosphere (Burke et al., 2019; Gautier et al., 2018; Crick et al., 2021; Baroni et al., 2008), but these analyses are still scarce for the last glacial period.

1.4 Extending the ice-core volcanic record into the last glacial period

Here we extend the ice-core record of sulfate deposition in Greenland and Antarctica by employing sulfate records from three Greenland and three Antarctic ice cores in the interval 60-9 ka (in one core we use elemental sulfur measurements, but for the sake of brevity we will refer to sulfate records). We investigate the sulfur emission strengths (i.e. defining the climate impact potential) and the frequency of volcanic eruptions detected in either Greenland or Antarctica. For eruptions identified in both hemispheres, we estimate the climate forcing against modern analogues and determine the occurrence of very large eruptions.

2. **Methods**

2.1 Ice-core records

For Greenland we used the North Greenland Eemian Ice Drilling ice core (NEEM) (Dahl-Jensen et al., 2013), the North Greenland Ice Core Project ice core (NGRIP2) (Andersen et al., 2004), and the Greenland Ice Sheet Project 2 ice core (GISP2) (Grootes et al., 1993), and in Antarctica the WDC ice core (WAIS Divide Project Members, 2013; 2015), the EPICA Dome C ice core (EDC) (EPICA community, 2004), and the EPICA Dronning Maud Land ice core (EDML) (EPICA community, 2006).

The sulfate records were obtained by different analytical methods and with different temporal resolution as detailed in the Table S1. For NGRIP the SO_4^{2-} concentration was obtained by a Continuous Flow Analysis system (CFA) (Bigler, Thesis, 2004; Röthlisberger et al., 2000). For WDC, sulfur was measured by ICP-MS coupled to a CFA system (Sigl et al., 2016). For EDC and EDML, SO_4^{2-} was measured by Fast Ion Chromatography (FIC) coupled to a CFA system (Severi et al., 2015). For GISP2 and for a second NGRIP profile, SO_4^{2-} was obtained from discrete samples by Ion Chromatography (IC) (Clausen et al., 1997; Mayewski et al., 1993; Siggaard-Andersen, PhD thesis, 2004). The temporal resolution of the sulfate records decreases with ice-core depth and ranges from sub-annual for the CFA profiles to decadal for the lower-resolution discrete profiles (Table S1 and Fig. S2). The high-resolution NGRIP and WDC records have been resampled to annual resolution, which we see as an upper limit for the effective resolution during the oldest part of the analysis in last glacial. As discussed in section 3.4, we are also resampling these records to lower resolution in order to obtain comparable resolution throughout the investigated period and in order to investigate eruption occurrences among stadial and interstadial periods. Minor data gaps were interpolated using linear interpolation and larger gaps are indicated as missing data. Sulfur and sulfate records were corrected for the sea-salt-sulfur contribution based on sodium concentrations as sea salt tracer by assuming 0.084 for the ratio of Na/S (Bowen et al., 1979), except for EDC. In all cases, the sea-salt correction is less than 15% of the measured sulfate background signal, giving a slight change to the non-sea-salt-sulfur. For the Holocene period, methanesulfonic acid (MSA) was applied for a minor correction of the Antarctic sulfur signal (Cole-Dai et al., 2021). As there are no continuous MSA records available for WDC over the investigated period, we do not make this correction here.

For the 12-9 ka interval, the Greenland sulfate deposition is based on the NGRIP and GISP2 records only, as the NEEM dataset is not available.

Apart from using the sulfate records, the depth assignment of the volcanic peaks was occasionally assisted by application of other high-resolution records that also are indicators of volcanic sulfate deposition. Those include the Electrical Conductivity Measurement (ECM) profile, the Di-Electric Profiling (DEP) and the liquid conductivity records, that are also available for most of the applied cores (Table S1 for a complete list of records and references).

2.2 Background signal determination and volcanic peak detection

To determine the biogenic sulfate background level of the ice-core sulfate records and detect volcanic peaks above this background, we apply robust peak detection methods similar to those applied for Holocene records (Fischer et al., 1998; Karlof et al., 2005; Gao et al., 2007; Sigl et al., 2013), which allow for a change with sulfate background variability over time. A running median filter with a width of 50-180 years was applied to estimate the non-volcanic background signal. Due to the different depth resolution of the individual records, and because of the highly variable and abruptly changing background levels of the Greenland sulfate levels across DO-events, it has been necessary to apply different filter widths for different records (Fig. S1 (a-y) and Table S1). A second iteration of a reduced running median (RRM) filter using the same filter widths was applied after removal of the spikes identified in the first iteration. For the coarse-resolution NGRIP IC sulfate record, a continuous background determination was not possible and the background has been estimated manually for selected events only.

For all records, a volcanic detection threshold was estimated as RRM plus three times the running median of absolute deviations from the RRM (RMAD) using the same window widths as for the background determination (Fig. S1 (a-y)). In Greenland, the RMAD value varies strongly across DO-events due to the much greater background variability during stadial periods as compared to interstadials (Table S2). This implies that the volcanic detection may be compromised for the time windows covering the fast transitions from stadials and interstadials (lasting on the order of decades to up to about 150 years, Capron et al. (2021)) when the background variability changes in a short time. Thus, the volcano frequency found in these short intervals may be impacted, but the volcanic frequency outside of these short intervals is not affected. The duration of a volcanic event is estimated from the fraction of the sulfate spike that is above the RRM and the sulfate deposition associated with the event is calculated by integrating the sulfate concentrations above the RRM across the duration of the event. The volcanic sulfate peak area S in kg km^{-2} is calculated as follows:

$$S = \int_{D1}^{D2} (y - RRM)dy * 0.917 \quad (1)$$

where y is the nss-sulfate concentration in units of ppb, 0.917 is the ice-water density in g cm^{-3}, and the sulfate layer in the ice core is constrained between the depths D1 and D2 in m ice equivalent. At shallow depth, the temporal duration of the sulfate deposition can be determined precisely, but in the last glacial period peak broadening by diffusion is hampering such a determination.

2.3 Correction for ice flow / layer thinning

As the volcanic layer is buried in the ice sheet, the layer is being thinned by ice flow. In order to calculate the amount of sulfate deposited on the ice sheet at the time of the eruption a correction for the thinning of the volcanic layer in the ice must be applied.

$$SF = \frac{S}{T} \quad (2)$$

Here SF is the accumulated sulfate flux in kg km^{-2} and T is the layer thinning (the ratio between the layer thickness in the ice core and the original layer thickness). The layer thinning has been calculated by site-specific ice-flow models (thinning function) that we applied here (Table S1 and Fig. S2 (c)). During the last glacial period, the layer thinning can be significant. For the Greenland cores, the thinning rate ranges from a 60% reduction of the original layer thickness (T=0.4) at 12 ka b2k to as much as 90% (T=0.1) at 60 ka b2k (Table S1). For Antarctica, the thinning rate is most significant for the high-accumulation WDC core, where it approaches 95% (T=0.05) at 60 ka b2k (Fudge et al., 2016; Buizert et al., 2015), whereas the EDC core exhibits a modest thinning of 30% (T=0.7) at 60 ka b2k (Fig. S2 (c)). For the WDC core, we apply the thinning function of Fudge et al. (2016) for the upper 2800 m, whereas below 2800m we apply a simple linear fit to the gas-based thinning function (Buizert et al., 2015) that has large and possibly unrealistic wiggles (Fig. S2 (c)). As the volcanic sulfate deposition scales with the amount of thinning, an inaccurate thinning factor has large implications for the calculated sulfate depositions.

For high snow accumulation sites, such as those in Greenland and coastal Antarctica, it is quite likely that wet deposition is dominating the sulfate deposition at present day (Kreutz et al., 2000; Schupbach et al., 2018). During the last glacial period, dry deposition may have played a more important role, giving rise to a potential bias of our glacial sulfate deposition estimates. We do not attempt to make any corrections for this effect.

2.4 Correction of volcanic signals for low resolution data

As the depth resolution of the sulfate records for the GISP2 and NEEM cores is relatively low (Fig. S2 (a)), adjacent acidity peaks may be merged into falsely large acidity spikes. We made a manual correction for this effect by comparing to the corresponding higher-resolution ECM and DEP records (depth resolution of 1 cm or higher) of the same core and removed or split falsely large peaks according to the associated ECM or DEP peaks. The specific correction for volcanic signals is indicated in Table S3.

2.5 Volcanic sulfate deposition records

We generate three lists of volcanic sulfate deposition for the 60-9 ka period: one for eruptions identified in the Greenland ice cores (Table S3), one for eruptions identified in the Antarctic ice cores (Table S4), and one for global (bipolar) eruptions identified in both Greenland and Antarctica (Table S5). The bipolar list contains the large global eruptions identified by Svensson et al. (2020) and also two large bipolar eruptions found in Veres et al. (2013) for the 12-9 ka period. Furthermore, two additional bipolar eruptions at 44.75 ka b2k and 44.76 ka b2k have been included, applying the same methods as described in Svensson et al. (2020). For the bipolar list, no bipolar eruptions could be unambiguously identified in the 24.5-16.5 ka period, not because they may not have existed but because ice core synchronization is very difficult in this period. Therefore, the list covers only an effective period of 43 ka. The list of NH volcanism contains all volcanic deposits larger than 20 kg km^{-2} in any of the applied Greenland ice cores, and the list containing the Southern Hemisphere includes all deposition events larger than 10 kg km^{-2} for the Antarctic ice cores, which biases our list to larger eruptions. This cut-off is necessary because of the highly variable sulfate background in the Greenland cold periods of the last glacial predominantly associated with mineral dust (e.g. gypsum (Svensson et al., 2000)) (Table S2). A sulfate deposition of 20 kg km^{-2} corresponds to half the Greenland deposition from the 1815 AD Tambora eruption (Sigl et al., 2015), thus only quite large events in terms of total sulfur injections into the atmosphere are detected in this work. If the cut-off is set at a lower value, a large number of presumably non-volcanic spikes will be identified in stadial periods. A similar cut-off applied to the sulfate deposition record of the last 2000 years (Sigl et al., 2013) reduces the number of identified eruptions in Greenland from 138 to 49 events. Likewise, for Antarctica, we are only identifying events that are referred to as ‘large’ or ‘very large’ by Cole-Dai et al. (2021). When eruptions are detected in several ice cores in Greenland or Antarctica, we provide the sulfate deposition value for each core, the range spanned by all the cores, and the calculated average sulfate deposition value. The average Greenland sulfate deposition is calculated by the simple mean of the three cores due to their similar sulfate-deposition levels and proximity of the ice coring sites (Fig. S3). In Antarctica, however, the ice-core

sites are far apart and the EDC core generally has the lowest sulfate deposition due to low snow accumulation or a reduced amount of sulfate reaching the remote EDC ice-coring site. Therefore, when there is only a sulfate signal present in one or two cores, the average sulfate deposition of Antarctica is calculated with a rescaling factor, similar to the method applied by Gao et al. (2008). The scaling factor is based on the relative ratio of sulfate deposition from the 30 largest eruptions (in terms of the sulfate deposition) in the three cores in the period of 60-9 ka. For the 30 largest eruptions identified in Antarctica, the ratio of the sulfate deposition among the three Antarctic cores is EDC:EDML:WDC =0.72:0.87:1.4 (Fig. S3).

The volcanic sulfate deposition uncertainty estimate is obtained from the error propagation in formula (1) and (2). For NGRIP, NEEM, GISP2 and WDC, we apply an estimated 21% uncertainty of the sulfate concentration levels independent of the analytical method (Fig. S3 (e)), an estimated 10% uncertainty of the applied thinning functions, and a 15% uncertainty related to the varying temporal resolution of the sulfate records. This leads to an error estimate of up to 26% for individual deposition events that we apply as error estimate for all the derived sulfate depositions. For EDC and EDML, the low accumulation leads to an additional large local variability in sulfate deposition of up to 29% (Gautier et al., 2016), so for those cores we arrive at an combined error estimate of 40% for individual deposition events. When there are sulfate signals from three ice cores in one hemisphere, we used the standard deviation of the rescaled volcanic sulfate depositions for all ice cores to estimate the uncertainty for the average area volcanic sulfate deposition. When there is a common signal in fewer than three cores, we use the maximum uncertainty of the volcanic sulfate deposition from the individual cores.

2.6 Latitudinal band assignment of bipolar volcanic eruptions

The volcanic sulfate deposition in Greenland and Antarctica shows a distribution pattern related to the latitudinal band of the eruption site (Fig. 1) (Marshall et al., 2019). To estimate the latitudinal band of bipolar volcanic eruptions of unknown origin, we applied the Support Vector Machine (SVM) classification model of Hastie et al. (2009) and Vapnik (1998). The classification model is based on a kernel function generation and logistic regression. The model was trained using 21 eruptions for which the eruption site is known from tephra deposits in the ice (Table S6). The input values for each eruption to the model are the average Greenland sulfate deposition, the average Antarctic sulfate deposition and the latitudinal band (above 40°N, 40°N-40°S, or below 40°S) of the eruption site. The cross-validation used for tuning the algorithm is 10-fold partition for each evolution. For an optimal classification, a maximum-margin hyperplane was used to separate two classes. The kernel scale and box constraints were chosen for the model and a Bayesian optimization was used to optimize the above two parameters to yield the best classification model (Fig. S4) (more details on this method in Hastie

et al. (2009), page 17). The bipolar eruptions of unknown origin were predicted into two latitudinal bands – above 40°N (NHHL) and below 40°N (LL or SH) (Table S5) based on the trained model. Due to the low number of known volcanoes erupted in the high latitudes of the Southern Hemisphere, the method does not allow unambiguous identification of eruptions potentially located in this region.

3 Results

3.1 The Greenland volcanic sulfate deposition record (60-9 ka)

The sulfate deposition records derived from the NGRIP, NEEM and GISP2 ice cores are displayed in Fig. 2 and Fig. S1 (a-y). The background level of the sulfate signal in the Greenland cores is in the range of 50-200 ppb with both the absolute level and the signal variability being much higher in stadial periods than in interstadial periods (Table S2). At the abrupt climate transitions during the last glacial period the sulfate background changes abruptly, making it difficult to determine the background level and volcanic detection limits (see Section 2.2). The higher background level and variability during the stadial periods is partly due to the lower snow accumulation during these periods.

Using a 20 kg km^{-2} deposition threshold, 1113 volcanic events are identified in Greenland in total (Table S3). Table S7 shows the number of volcanoes detected from one, two or three Greenland ice cores, respectively. NGRIP has the highest event detection rate because of its superior depth resolution. Depth resolution becomes increasingly critical in the cold climate of the investigated period where annual layers get down to a few centimeters of layer thickness (Fig. S2 (d)).

The difference in sulfate deposition among the cores reflects to some degree the spatial variability in sulfate deposition within Greenland, but is also strongly influenced by the sulfate record type (IC, FIC, CFA), the data resolution, the thinning correction made for each site, and possibly the accumulation rates. A comparison of the sulfate deposition between NGRIP, NEEM and GISP2 for the 30 largest volcanoes with identified signals in Antarctica ice cores shows that there is a very large spread in the signal from event to event (Fig. S3 (a-d)). Due to the large variability of sulfate deposition values among the cores, we provide the full range of sulfate deposition values spanned by the cores as well as the average sulfate deposition value, when an eruption is identified in several ice cores.

Fig. S3 (e) shows a comparison between the 57 largest volcanic events identified in the NGRIP ice core, as derived from the high-resolution CFA SO_4^{2-} record and from the lower resolution IC SO_4^{2-} record, respectively (Table S5). This comparison illustrates the differences in calculated sulfate depositions due to the analytic

315 method and record resolution only, as the sulfate deposition and the thinning factor uncertainties are eliminated. It is obvious from the comparison that the derived sulfate deposition of a single event in a single core should not be taken at face value; there are very large uncertainties on top of the variability caused by the spatial distribution pattern. Still, being the first systematic compilation of large volcanic eruptions from the last glacial period, the estimated depositions provide a good estimate of the order of sulfur emission strength and the
320 frequency of large volcanic eruptions in Greenland.

Out of the 1113 volcanic events identified in Greenland we identify 10 very large events with sulfate deposition estimated to be larger than 300 kg km^{-2} – where 9 have an Antarctic counterpart indicating their global impact. We identify 87 volcanic events with sulfate deposition larger than 135 kg km^{-2}, thereby exceeding the Icelandic Laki eruption occurring in 1783 CE, which produced the largest Greenland sulfate deposition in the last 2500
325 years (Sigl et al., 2015). The largest sulfate deposition in Greenland is by far the North Atlantic Ash Zone (NAAZ II) event occurring at 55.38 ka b2k (Rutledal et al., 2020; Austin et al., 2004). The sulfate deposition of this event is in the range of 866-1436 kg km^{-2}, which is more than a factor of two higher than any other event occurring in the investigated period. The second largest event is an unknown eruption occurring at 45.55 ka b2k with a sulfate deposition in the range 200-849 kg km^{-2}. Those and other large events will be discussed in more
330 details in section 4.4.

3.2 The Antarctic volcanic sulfate deposition record (60-9 ka)

The volcanic sulfate deposition extracted from the EDML, EDC and WDC ice cores are shown in Fig. 2 and Fig. S1 (a-y). The sulfate background level in Antarctica is comparable to that of Greenland (Table S2), but there is much less signal variability and an absence of abrupt shifts associated with Greenland DO transitions,
335 making volcanic signal detection more robust. In total, 740 (350) volcanic sulfate deposition values estimated to be larger than 10 (20) kg km^{-2} are identified in the Antarctic ice cores (Table S4 and Table S7). WDC has the highest accumulation of the three records, but as the deepest part of the applied WDC record is close to bedrock, layer thinning becomes very significant here (Fudge et al., 2016) (Table S1). Therefore, in the deepest section of the WDC core, fewer eruptions are detected as compared to EDML and EDC, and the derived WDC sulfate
340 deposition has a very strong dependency on the applied thinning function. EDC has the lowest accumulation of the three and also the lowest temporal resolution of the sulfate record. Therefore, smaller events are generally not detected in the EDC core, and the low accumulation contributes to some eruptions being partly or entirely absent from the record (Gautier et al., 2016).

The volcanic deposition of the 30 largest events in Antarctica are compared among the cores in Fig. S3. In general, there are large differences among the sulfate deposition in the different cores for the same events, primarily owing to the large gradient of accumulation rates and spatially different transport pathways over Antarctica (Sigl et al., 2014). The influence of different analytical techniques (FIC or CFA-ICP-MS) and the temporal resolution of the records may also accounts for some of the variability, as well as post-depositional processes (Gautier et al., 2018).

In the 60-9 ka period, there are 31 large volcanic events with a sulfate deposition larger than 78.2 kg km^{-2}, which is the largest volcanic deposition in Antarctica over the most recent 2500 years (Sigl et al., 2015). Forty-eight volcanic events have a sulfate deposition larger than 64 kg km^{-2} corresponding to the Antarctic sulfate deposition of the Kuwae 1458 CE eruption (Sigl et al., 2015). Among the 50 largest eruptions, 28 are also identified in Greenland ice cores. The largest volcanic signal detected in Antarctica is occurring at around 46.69 ka b2k with a sulfate deposition of 121.0-369.4 kg km^{-2}.

3.3 The bipolar volcanic sulfate deposition record (60-9 ka)

For the 60-9 ka period, the 85 bipolar volcanic eruptions that have been identified in both Greenland and Antarctic ice cores (Veres et al., 2013; Svensson et al., 2020) are listed separately in Table S5. We note that no bipolar eruptions have been identified in the interval 24.5-16.5 ka, because of the general difficulty to synchronize ice cores in this period (Seierstad et al., 2014). Twenty-eight out of the 85 bipolar eruptions have been identified in all six ice cores. Two of the bipolar volcanic eruptions are known from Greenland ice-core tephra deposits to be of Icelandic origin: The Vedde ash eruption (12.17 ka b2k) (Mortensen et al., 2005) and the NAAZ II eruption (55.38 ka b2k) (Rutledal et al., 2020). Furthermore, there are tephra deposits in Greenland from the Japanese Towada-H eruption (ca 15.68 ka b2k) (Bourne et al., 2016). In Antarctica there is tephra deposited from the New Zealand Oruanui, Taupo, eruption (ca 25.32 ka BP1950) (Dunbar et al., 2017) (Table S6). For the bipolar eruptions the volcanic forcing can be estimated using methods previously applied to Holocene eruptions (see section 4.3).

3.4. Relationship between data resolution and the volcanic eruption record of the last glacial (60-9 ka)

To investigate the frequency of different size categories of volcanic eruptions over time, we need to consider the sample resolution of the underlying sulfate records (Fig. S2 (a+b)). As we go back in time, the layer thinning becomes stronger which makes it increasingly difficult to detect smaller eruptions signals. Depending on the ice-core sample resolution, the apparent number of smaller eruptions decreases relatively faster with increasing

age (or depth) than the larger eruptions, as the former will no longer exceed the detection threshold determined by the background signal due to smoothing of the records (Fig. S5). The effect is seen when the frequency of detected eruptions is separated into fractions of sulfate deposition sizes. We separated the eruptions according to the 0.7 and 0.9 quantiles of the volcanic sulfate deposition distribution, which for Greenland are 68 kg km^{-2} and 140 kg km^{-2} and for Antarctica are 25 kg km^{-2} and 50 kg km^{-2}. When considering the frequency of volcanic eruptions across the investigated period, we should preferably have the same or at least a comparable temporal sulfate sample resolution throughout the period in order to minimize this age (or depth) bias.

For Greenland, only the NGRIP sulfate record has high (sub-annual) resolution for most of the investigated interval (Fig. S2 (b)). Therefore, the number of eruptions detected in different periods will depend strongly on the NGRIP sample resolution. The NGRIP sulfate has an effective resolution of 8-20 mm due to smoothing of the record in the ice and – most importantly – by signal dispersion during the measurement. Using an approach similar to that of Rasmussen et al. (2005), we performed a spectral analysis of the NGRIP sulfate record to determine a signal cut-off of around 2 cm, which is comparable to that of other components analyzed with the same setup (Bigler et al., 2011) (Fig. S6). Two cm corresponds to about 2 annual layers in NGRIP in the climatically coldest and oldest sections of the investigated interval. In Table S8 and Fig. S5 we investigate the effect of increased smoothing of the NGRIP sulfate record for the detection of sulfate spikes. As expected the number of detected eruptions decreases with increased smoothing, however, with 3 years smoothing, the number of larger sulfate spikes starts to increase as adjacent sulfate peaks are being merged.

As a compromise between compensating for the decreasing resolution of the record with depth and at the same time avoiding a strong influence of the peak merging effect, we smoothed the NGRIP sulfate record to 2-year resolution for the eruption frequency analysis, knowing that this is eliminating a fraction of the smaller eruptions in the younger section of the record. With the 2-year smoothing there is probably still a bias towards a higher detection rate in the stadial periods due to the high signal variability of the sulfate record in those periods (see discussion in section 4.1). The GISP2 sulfate record has lower than 10-year resolution in the 60-14 ka period (Fig. S2), so in this period we can only use the GISP2 sulfate record to estimate the sulfate deposition of the larger eruptions. The NEEM sulfate record has a constant resolution of 10 years and we use this record throughout the investigated period. In Fig. 3 we show the records of detected Greenland eruptions per millennium with the sulfate deposition grouped into three size fractions.

For Antarctica, EDML and EDC have fairly constant thinning rates for the 60-9 ka period (Fig. S2 (c)), whereas WDC has very strong thinning in the oldest part of the period, due to the high accumulation rate (Fig. S2 (c)). Spectral analysis of the Antarctic sulfate records shows the effective resolution (Table S1) and the signal cut-off

is around 2 cm, 3 cm, and 1 cm for EDML, EDC and WDC, respectively (Fig. S6). In order to have comparable resolution throughout the investigated period, we smoothed the entire WDC sulfate record to 2-year resolution to homogenize the record resolution across the investigated period. For EDML the corresponding effective signal resolution is 1-2 year for the entire period, so we keep the original resolution of the EDML sulfate record for the entire period. The EDC sulfate record has almost constant resolution, so we apply this record throughout the investigated period. The result of the frequency analysis is discussed in section 4.1.

4. Discussion

In the following we investigate possible climate-volcano links on different time scales, estimate the last glacial volcanic forcing, and compare the glacial volcanic record to that of the last 2500 years. Many studies have discussed a possible impact of climate on the frequency and magnitude of volcanic eruptions (Cooper et al., 2018). In particular, the melting of the large ice sheets at the end of the last glacial period and the corresponding sea-level rise are thought to have created crustal stress imbalances and increased the volcanic eruption frequency in that period (Watt et al., 2013; Huybers and Langmuir, 2009; Zielinski et al., 1996; Zielinski et al., 1997).

4.1 Millennium scale volcanic eruption variability

We investigate the variability in eruption frequency and sulfur emission strength with the DO cycles by separating the detected volcanic eruptions according to climate of 'cold' and 'milder' periods, applying the onset and termination of DO events defined by Rasmussen et al. (2014). 'Cold' periods constitute the stadial periods from 21 ka b2k to 60 ka b2k, covering a total of 21.8 ka. 'Mild' periods are the remaining periods that include all of the interstadial periods from 21 ka b2k to 60 ka b2k, adding up to 17.2 ka years. We grouped the detected eruptions according to the size of deposited sulfate and also investigated the effect of smoothing the NGRIP sulfate record to 1, 2, 3, and 5 years resolution (Fig. S7). For Antarctica, the number of detected eruptions (per millennium) is very similar for stadial and interstadial periods, independent of deposition size categories and record smoothing (Fig. 4). For Greenland, however, the number of volcanic eruptions is higher in stadial periods than in interstadial periods (Fig. 4), in the smaller deposition category (20-68 kg km^{-2}) this effect decreases with increasing NGRIP sulfate record smoothing (Fig. S7).

This observed difference leaves us two options: either there is a true millennium-scale volcanic eruption variability related to northern hemispheric climate variability during the last glacial period, or the dependency is an artefact caused by the very different properties of the Greenland sulfate record in stadial and interstadial

periods. In Greenland, the variability of the sulfate background level is high in cold periods, stadials and the LGM, and low in milder periods such as interstadials (see section 3.1). We try to take this difference into account by employing the variability-dependent RMAD to determine the eruption detection limit, but because of the very different character of the sulfate profiles in cold and milder periods there is still the possibility of having a climate related detection bias of sulfate spikes that is unrelated to the actual volcanic eruption record. For example, in cold periods, it could be that strong seasonal sulfate spikes associated with marine or terrestrial (non-volcanic) sulfate production could be detected as smaller volcanic eruptions. For recent times, Gao et al. (2007) has demonstrated that the volcanic sulfate deposition to some degree is accumulation dependent, with increased accumulation leading to higher sulfate deposition. Since, however, the highest accumulation occurs in the interstadial periods, this effect would lead to relatively higher sulfate deposition in interstadial periods, which is the opposite of what is observed.

We investigated the effect of a possible seasonal sulfate contributions of non-volcanic origin by a smoothing exercise where successively increased smoothing of the NGRIP sulfate record increasingly eliminates the detection of smaller short-lived (seasonal) sulfate spikes. Fig. S5, Fig. S7 and Table S8 show the number of sulfate spikes detected in stadial and interstadial periods as a function of the degree of smoothing. It is seen that for cold periods, the number of detected small and short-lived sulfate spikes decreases significantly with increased smoothing, whereas the effect is almost absent for milder periods. This suggests that the higher number of detected sulfate spikes in cold periods is mainly due to spikes of periodic duration of sulfate background which we believe are less likely to be of volcanic origin. For volcanic eruptions that are large enough to inject sulfate into the stratosphere modern observations show that the sulfate fallout typically will last several years. We thus conclude that the apparent increased volcanism detected in cold periods is most likely an artefact caused by non-volcanic seasonal contributions from high-sulfate marine or terrestrial sources. It could for example be contributions from gypsum that is known to have high deposition fluxes in Greenland during stadial periods (Legrand and Mayewski, 1997). Indeed, for bipolar events we do observe a higher correlation in stadial periods than in interstadial periods between the volcanic sulfate deposition and both insoluble dust concentration and sodium concentration (Fig. S10). We cannot exclude, however, that other mechanisms such as different atmospheric circulation patterns, or different sulfate deposition process in terms of dry versus wet deposition, are also affecting the Greenland volcanic detection rates in stadial versus interstadial periods. We note that because an increased smoothing of the sulfate record mostly decreases the number of smaller detected sulfate depositions, the effect of smoothing on the large accumulated sulfate deposition over time is less important (Fig. S5 and Table S8).

4.2 Long-term volcanic eruption variability

In order to estimate the long-term pattern of volcanic activity, the accumulated number of volcanic eruptions and resulting sulfate deposition in Greenland and Antarctica over the investigated period are compared in Fig. 5 (same data as applied in Fig. 2). The cumulative volcanic number (sulfate deposition) in Greenland is larger than in Antarctica by a factor of 3.2 (4.7), considering only sulfate depositions larger than 20 kg km^{-2} at both poles. We attributed this mainly to the larger number of volcanoes situated in the NH, but it is possibly also related to the proximity of Iceland to Greenland and to other volcanic regions located upwind of Greenland, as well as to the differing atmospheric circulation patterns between the two hemispheres (Toohey et al., 2019). In terms of cumulated volcanic number there is some temporal variability that could be climate related, but overall the eruption frequency is rather constant in comparison to the geological record from Large Magnitude Explosive Volcanic Eruptions (LaMEVE) database (Brown et al., 2014), most likely because the ice-core preservation and identification are much more homogeneous over time than that of radiometrically dated eruptions.

The number of volcanic eruptions per millennium shows a fairly constant level both for Greenland and for Antarctica (Fig. 3, Fig. S8 and Fig. S9). The Early Holocene increase in global volcanism as suggested by Watt et al. (2013) is not identified in our record. Neither is the periodicity of Campanian eruptions as identified by Kutterolf et al. (2019), but this pattern could be masked by eruptions from elsewhere.

Based on the EDC sulfate record, Castellano et al. (2004) determined the Antarctic volcanic sulfate deposition to be fairly constant over the last 45 ka, except for an increase during the last 2000 years. The eruption frequency level of 5-10 eruptions per millennium determined in that study is on the low side compared to the present study, in particular for the older part of the period (Fig. 3). This is likely because the EDC sulfate record has low resolution and could not pick up all of the smaller short-lived eruptions, also because the low accumulation at the EDC site does not record some eruptions (see methods/results section). Over the 60-9 ka interval we have detected 224 volcanic eruptions in EDC as compared to 513 and 496 in the higher resolution WDC and EDML records, respectively (Table S4).

Recently, Cole-Dai et al. (2021) compiled a Holocene volcanic record from the high-resolution sulfate record of the high-accumulation WDC ice core. The authors determine a fairly constant Holocene volcanic activity with identification of 426 eruptions of which 162 and 44 have sulfate depositions larger than 10 kg km^{-2} and 30 kg km^{-2}, respectively. Those numbers are very comparable to our findings for Antarctica in the period of 11-9 ka (Fig. 3).

Based on the same GISP2 sulfate dataset as applied in the present study and after introducing a rescaling to compensate for the decreasing sample resolution with depth, Zielinski et al. (1996, 1997) identified an enhanced

northern hemispheric volcanic eruption frequency in the deglacial period (17-6 ka) compared to the 60-0 ka average. In our 3-core Greenland sulfate deposition compilation, we also found an increased volcanic eruption frequency over the deglacial period, which is 34% higher than the late Holocene period (2-0 ka), especially for the fraction of large sulfate deposition events (Fig. 3 and Fig. 4). In Antarctica, neither the detected eruption frequency nor the total sulfate deposition over the deglacial period are higher than the average for the full 60-9 ka interval. We therefore conclude that the increased number of large eruptions occurring in the deglacial period are mostly of northern hemispheric origin. This hypothesis is supported by the elevated number of tephra deposits identified in Iceland records (Maclennan et al., 2002) and in Greenland during the deglacial period mostly of Icelandic origin, a few from Japanese and unknow origins (Bourne et al., 2016; Zielinski et al., 1997; Mortensen et al., 2005; Gronvold et al., 1995). Van Vliet-Lanoe et al. (2020) found that the enhanced volcanic activity in southern Iceland is most likely related to stress unlocking during deglaciation events and related to rifting events at the melting margin of the ice sheet. In the period of 14.6-13.1 ka in Southeast Alaska, an enhanced volcanic activity from the Mount Edgecumbe Volcanic Field has also been observed by Praetorius et al. (2016).

For the glacial period (60-21 ka), the frequency of detected eruptions is similar to that of the last 2000 years, when comparing the same sulfate deposition fractions (Fig. 4). We note that for the last 2000 years only eruptions with sulfate depositions larger than 20 kg km^{-2} are included and in order to make the profiles comparable - the sulfate records have been smoothed with a two-year filter. The apparent increase in global volcanism over the last millennia in the geologic records (Brown et al., 2014) is therefore most likely due to an under-representation of older eruption identifications in that study (Papale, 2018; Deligne et al., 2010). When it comes to sulfur emission strengths of eruptions and accumulated sulfate deposition, however, the last 2000 years appear to be under-represented in very large eruptions as compared to long periods of the last glacial period (Table 1).

4.3 Estimating the volcanic forcing of the last glacial 60-9 ka

To estimate the volcanic radiative forcing from eruptions occurring in the last glacial and early Holocene we need to (i) constrain the sulfate stratospheric aerosol loading (we applied the method of Gao et al. (2007)), (ii) convert the stratospheric aerosol loading into the global mean stratospheric aerosol optical depth (SAOD) (we applied the methods of Crowley and Unterman. (2013) and that of Aubry et al. (2020)), and (iii) convert global mean SAOD to the global mean radiative forcing (we applied the methods of Hansen et al. (2005) and that of Marshall et al. (2020)). The global stratospheric sulfate aerosol loading requires a separation of NH high-latitude

eruptions from other eruptions, as the two eruption groups are scaled differently (Gao et al., 2007). We defined NH high latitude eruption as eruptions that occurred at a latitude above 40° N. To identify the NH high latitude eruptions, we applied a Support Vector Machine learning classifier model (SVM – see methods section), that is trained by the bipolar sulfate deposition of volcanic eruptions for which the eruption site is known. We applied 17 Holocene and 4 glacial volcanic eruptions of known origin (Table S6) to predict that 50 out of 85 bipolar eruptions of unknown origin are likely to have occurred in the NH high latitudes (Fig. 1 and Fig. 6). We then reconstruct the volcanic radiative forcing using three different approaches:

1) The global mean SAOD is obtained using the method of Crowley and Unterman. (2013) and the radiative forcing calculation applies the scaling factor of Hansen et al. (2005). Here the volcanic radiative forcing is calibrated against Pinatubo 1991 AD (at 15°N). This approach is similar to the one used by Sigl et al. (2015).

2) The global mean SAOD is obtained using the scaling factor of Aubry et al. (2020) and the radiative forcing calculation applies the scaling factor of Hansen et al. (2005). This approach is similar as IPCC AR5.

3) The global mean SAOD is obtained using the scaling factor of Aubry et al. (2020) and the radiative forcing calculation applies the scaling factor of Marshall et al. (2020), which considers rapid aerosol adjustment for large volcanic eruptions.

All of the reconstructed volcanic radiative forcings are calibrated and evaluated based on modern volcanic eruptions, and they are therefore potentially biased when applied to the eruptions occurring in the very different glacial climate (see section 4.1). Table S5 and Fig. S11 present the reconstructed volcanic radiative forcing of individual volcanic events using the three approaches. The reconstructed volcanic forcing obtained by methods 2) and 3) is significantly weaker than that obtained by method 1) by a factor of 1.3 and 2.8, respectively, when integrated over all events. In the following, we adopt method 3) to present the reconstructed volcanic forcing values.

Having estimated the volcanic forcing of the glacial and early Holocene eruptions, we can compare it to the well-constrained eruptions that occurred over the last 2500 years (Sigl et al., 2015). In Table 1 we compare the number of eruptions with a climate forcing larger than Oruanui, Taupo, 25.32 ka BP1950; the unidentified eruption of 426 BC, and Tambora, 1815 AD for the periods of 2.5-0 ka, and 60-9 ka. Note that the investigated period of the last glacial and the early Holocene covers some 43 ka (60-9 ka minus the section of no identified bipolar eruptions 24.5 to 16.5 ka). Among the 85 bipolar events investigated in the last glacial and early Holocene, three eruptions are found to be larger than Oruanui, Taupo, and 25 eruptions are found to be larger than the largest eruption of the past 2500 years.

Based on geological evidence, the occurrence of large volcanic eruptions was estimated in terms of their VEI (Volcanic explosivity index), which is based on the volume of ejected magma. The average occurrence rate of VEI-7 (VEI-8) volcanoes discovered in the last 125 ka BP (2600 ka BP) is 0.3 (0.01) per millennium, respectively, based on databases of LaMEVE and GVP (Papale, 2018). From ice-core records, we cannot directly derive the VEI index, but the estimated volcanic radiative forcing is likely to be another good indicator of volcanic eruption magnitude. The average rate of volcanoes in the 60-9 ka interval with a climate forcing larger than the 1815 AD Tambora eruption (VEI-7) is 1.60 per millennium (Table 1). In the same interval, we have 4 eruptions with a climate forcing larger or equal to the 25.32 ka BP1950 Taupo Oruanui (VEI-8) eruption. Of those, the Icelandic 55.38 ka NAAZ II volcanic event is likely to be overestimated due to its proximity to Greenland (see section 4.4.). Thus, we identify three eruptions with a climate forcing larger than or equal to Taupo Oruanui 25.47 ka, occurring at a rate of 0.07 eruptions per millennium. Those ice-core based eruption frequency estimates are thus about 5.3 times larger than those based on geological evidence for Tambora 1815 AD, and 7 times larger as Taupo Oruanui 25.32 ka BP1950 resting on the observation that there exists a positive relationship between the volume of ejected magma and the emission of sulfur gas for a volcanic eruption (Table S6).

4.4 Large and notable volcanic eruptions of the last glacial period (60-9 ka)

The largest eruptions of the last glacial period and early Holocene are ranked by the average climate forcing in Table 2. The highest ranking on the list is the Icelandic eruption associated with the NAAZ II occurring in GS-15.2 at 55.4 ka b2k (Gronvold et al., 1995; Zielinski et al., 1997). The sulfate deposition in Greenland from this eruption is enormous (almost 15 times higher than the deposition for Laki 1783 AD), but none or only very little sulfate is deposited in Antarctica. With its close proximity to Greenland, it is therefore likely that a large fraction of the sulfate was transported to Greenland through the troposphere and thus the estimated climatic forcing of –15.9 W m^{-2} is probably overestimated and should not be taken at face value. From the marine sediment records, the NAAZ II layer consists of different Icelandic events (Rutledal et al., 2020). For the above reasons, the eruption should not be considered as the largest eruption of the last 60 ka in a global context. The very wide range of sulfate deposition of 866.2-1435.6 kg km^{-2} among the Greenland ice-core records (Table S5) is probably due to a combination of 1) a true geographical variability in deposition in Greenland, 2) the quite significant and possibly inaccurate correction for layer thinning at great depth in the ice cores for this eruption, and 3) an unexplained difference related to the different analytical methods applied (see results section).

The second largest event on the list occurred in GI-12 at 45.56 ka b2k and is identified in all Greenland and Antarctic ice cores, but the deposition at EDC is very low, most likely due to its low accumulation and the low time-resolution of the sulfate record. The eruption is of unknown origin, but based on its relative Greenland and Antarctic sulfate deposition, it occurred in the NH extratropical area and its climate forcing is estimated to be -15.0 W m^{-2}.

Number three on the list of large eruptions occurred at 38.13 ka b2k; 100 years after the onset of GI-8 and 11 years before the occurrence of the Faroe Marine Ash Zone III (FMAZ III) tephra in Greenland (Davies et al., 2012). The eruption is detected in all ice cores (but there is a data gap for the WDC sulfur in this interval), and with very similar Greenland and Antarctic sulfate depositions this is most likely a low-latitude eruption with an estimated average climate forcing of -13.6 W m^{-2}, about 2 times that of Tambora (1815 AD).

The forth largest bipolar ice-sheet sulfate deposits are from the New Zealand Taupo, Oruanui, eruption that occurred in GS-3 at 25.32 ka BP1950, verified by the presence of a tephra deposit in Antarctica (Dunbar et al., 2017). The estimated average climate forcing of the eruption is -13.2 W m^{-2}, about 1.5 times that of Samalas 1257AD (-9.1 W m^{-2}) (Sigl et al., 2015), which caused large variability of atmospheric temperature of global climate for several years (Lim et al., 2016), prolonged the drought in North American and leading to the famine (Herweijer et al., 2007). Despite its magnitude, the sulfate deposition of the eruption is undetected in the Greenland GISP2 ice core, which has the lowest temporal sulfate-data resolution of all the used cores in this time period.

In GS-5.1 at 29.68 ka b2k there is a pair of volcanic eruptions separated by some 40 years, of which the younger event ranks seventh on the list of the largest eruptions. The estimated climatic forcing of this eruption is -12.5 W m^{-2} and it has a clear NH signature in the bipolar sulfate distribution. There is no associated tephra deposit in the ice cores, but we speculate the event originates from the Italian Campi Flegrei Y-3 eruption, being the only bipolar volcanic eruption of that magnitude within a range of several millennia. The Y-3 eruption is independently Carbon-14 dated to 29.0 ka b2k (Albert et al., 2015).

Number 8 on the list of the largest eruptions occurred at 46.68 ka b2k in GI-12 and is the only eruption in this study apart from the 25.32 ka BP1950 Taupo, Oruanui, eruption that has a clear southern hemispheric origin. The Antarctic sulfate deposition of the eruption is approximately twice that in Greenland (Fig. 1) and the eruption has an average estimated climatic forcing of -12.3 W m^{-2} or about 0.9 times that of Oruanui.

Right after the onset of GS-9 at 39.92 ka b2k there is another pair of large eruptions separated by some 46 years. Those are ranking respectively number 14 (39,915 a b2k; -10.6 W m^{-2}) and number 38 (39,869 a b2k; -8.8 W m^{-2}) of the large eruptions listed in Table 2. Both eruptions have bipolar sulfate distributions suggesting a NH eruption. Because of their magnitude and their stratigraphic setting right at the onset of GS-9 these volcanic events are both possible candidates for the Italian Y-5 Campanian Ignimbrite eruption. There is no tephra evidence for this suggestion in the ice cores, but tephra from this eruption has been identified in the Black Sea in very similar stratigraphic setting at the onset of GS-9 and the eruption is independently dated by Ar/Ar to 39.9 ± 0.1 ka b2k (Giaccio et al., 2017).

In the late GI-1 right before the onset of GS-1 / Younger Dryas there is a quadruple of bipolar eruptions covering a period of 110 years (Svensson et al., 2020). The oldest (13,028 a b2k; -10.5 W m^{-2}) and the youngest (12,917 a b2k; -10.0 W m^{-2}) of those eruptions are number 16 and 17 on the list of large eruptions. Both eruptions are likely to have occurred in the NH at above 40°N. The 12,917 b2k eruption has been suggested as a candidate for the Laacher See Eruption (LSE) that occurred in the East Eifel region in present-day Germany (Brauer et al., 1999; Baldini et al., 2018), but no tephra has been identified in the ice cores from this eruption. A recent publication, however, suggested that the LSE was around 130 years older (Reinig, et al., 2021) and is synchronous instead (within age uncertainty) with the oldest event of this quadruple of bipolar eruptions, but also with some minor sulfate signals. Stratospheric sulfur injections and changes in aerosol optical depth have recently been independently estimated in the late GI-1 based on a subset of four ice cores with less stringent cut-off criteria (Abbott et al., 2021) indicating this time period experienced stronger volcanic forcing than any other comparable period during the Common Era.

The Vedde Ash layer (number 36 in Table 2) originates from a significant euption from Katla, Iceland with widespread tephra deposition in Greenland (Mortensen et al., 2005; Gronvold et al., 1995) and the North Atlantic region in the middle of GS-1 / Younger Dryas at 12.17 ka (Lane et al., 2012). Surprisingly, this Icelandic eruption not only deposited large amounts of sulfate in Greenland but also a much smaller amount in Antarctica, where it is identified in the WDC and EDML sulfate profiles suggesting that it had a large stratospheric injection. The average volcanic forcing is estimated to about -8.8 W m^{-2}, but this value has to be taken with the caution as some of the sulfate could have made it to Greenland through the troposphere.

5 Conclusion

We have employed three Greenland and three Antarctic sulfate/sulfur ice-core records to document the global volcanic activity over the period 60-9 ka b2k. Detection of volcanic signals in the last glacial is challenging due to extensive layer thinning of the ice cores with depth and a highly variable sulfate background level in the Greenland ice cores across DO events. Due to those challenges, we limited ourselves to identify Greenland (Antarctica) eruptions with sulfate deposition larger than 20 (10) kg km^{-2}, which for Greenland is about half the volcanic sulfate deposition of the Tambora 1815 AD and for Antarctica comparable to the Pinatubo 1991 AD eruption.

With those restrictions we identified 1113 volcanic eruptions in Greenland and 740 volcanic eruptions in Antarctica verifying the NH to be the most volcanic active. Of those, 85 volcanic eruptions had global impact (bipolar volcanos) as they were previously identified in Greenland and Antarctic ice-core records. Compared to the past 2500 years, the ratio of bipolar volcanoes to total identified volcanic events is very low in last glacial period, highlighting the challenges of robust synchronization over the glacial period. Based on the hemispheric partitioning of sulfate deposition following well-known historical eruptions, we determined if the bipolar volcanoes are likely to be situated above or below 40 ° N latitude. We then estimated their climatic impact potential in terms of radiative forcing based on established methods. Throughout the investigated period, we find that 69 volcanoes are larger than the Tambora 1815 AD eruption, and one unknown volcano occurring at 45.56 ka b2k in the NH and one unknown volcano at 38.13 ka b2k in low latitude or in the Southern Hemisphere are larger than the Taupo, Oruanui, eruption occurring at 25.32 ka BP1950 in present day New Zealand. The Icelandic NAAZ II eruption (55.38 ka b2k) has by far left the largest sulfate deposition in Greenland, but due to its minor sulfate deposition in Antarctica, it is thought that only a fraction of the sulfur gases was injected into the stratosphere. In general, we observe significantly higher occurrences of very large eruptions (VEI 7 or larger) than estimated from the geological record, indicating that ice cores provide a more complete picture of volcanic activity in the past.

Overall, the frequency of volcanic eruptions per millennium is rather constant throughout the investigated period and comparable to that of the most recent millennia. In agreement with previous studies, however, we find elevated levels of volcanic activity in the NH during the deglacial period (16-9 ka b2k). In particular, many very large eruptions occurred in this interval, quite likely associated with the redistribution of mass related to the melt down of the major glacial ice sheets in this period. In contrast, an apparent increase of Northern Hemispheric volcanic activity in cold stadial periods as compared to milder interstadial periods is likely to be an artefact due

to the highly variable nature of the Greenland sulfate signal of those periods. It is unlikely to be related to the sea level variations occurring in parallel to stadial/interstadial changes, which are much smaller than the sea level increases that occurred over the glacial termination.

Data availability: The high-resolution NGRIP CFA sulfate dataset is available as supplementary information for this publication. All other applied datasets are available elsewhere.

Author contributions: Initial idea was designed by A.S.. Datasets were collected by A.S. and J.M.L.. J.M.L. analysed the data and created the figures. J.M.L. and A.S. prepared the manuscript. All authors contributed to the discussion and commented on the manuscript.

Competing interests: The authors declare no competing interests.

Acknowledgements: A.S., C.H., J.P.S., B.M.V., S.O.R. and D.D.J. were supported by the IceFlow grant (grant no. 00016572) from the Villum Foundation. J.M.L. is supported by a grant from the China Scholarship Council (grant no. 201904910426).

References

Abbott, P. M. and Davies, S. M.: Volcanism and the Greenland ice-cores: the tephra record, Earth-Science Reviews, 115, 173-191, 10.1016/j.earscirev.2012.09.001, 2012.

Abbott, P. M., Niemeier, U., Timmreck, C., Riede, F., McConnell, J. R., Severie, M., Fischer, H., Svensson, A., Toohey, M., Reinig, F., Sigl, M.: Volcanic climate forcing preceding the inception of the Younger Dryas: Implications for tracing the Laacher See eruption, Quaternary Science Reviews, 274, 1-9, 10.1016/j.quascirev.2021.107260, 2021.

Albert, P. G., Hardiman, M., Keller, J., Tomlinson, E. L., Smith, V. C., Bourne, A. J., Wulf, S., Zanchetta, G., Sulpizio, R., Muller, U. C., Pross, J., Ottolini, L., Matthews, I. P., Blockley, S. P. E., and Menzies, M. A.: Revisiting the Y-3 tephrostratigraphic marker: a new diagnostic glass geochemistry, age estimate, and details on its climatostratigraphical context, Quaternary Science Reviews, 118, 105-121, 10.1016/j.quascirev.2014.04.002, 2015.

Andersen, K. K., Azuma, N., Barnola, J. M., Bigler, M., Biscaye, P., Caillon, N., Chappellaz, J., Clausen, H. B., DahlJensen, D., Fischer, H., Fluckiger, J., Fritzsche, D., Fujii, Y., Goto-Azuma, K., Gronvold, K., Gundestrup, N. S., Hansson, M., Huber, C., Hvidberg, C. S., Johnsen, S. J., Jonsell, U., Jouzel, J., Kipfstuhl, S., Landais, A., Leuenberger, M., Lorrain, R., Masson-Delmotte, V., Miller, H., Motoyama, H., Narita, H., Popp, T., Rasmussen, S. O., Raynaud, D., Rothlisberger, R., Ruth, U., Samyn, D., Schwander, J., Shoji, H., Siggard-Andersen, M. L., Steffensen, J. P., Stocker, T., Sveinbjornsdottir, A. E., Svensson, A., Takata, M., Tison, J. L., Thorsteinsson, T., Watanabe, O., Wilhelms, F., White, J. W. C., and Project, N. G. I. C.: High-resolution record of Northern Hemisphere climate extending into the last interglacial period, Nature, 431, 147-151, 10.1038/nature02805, 2004.

Aubry, T. J., Toohey, M., Marshall, L., Schmidt, A., & Jellinek, A. M. (2020). A New Volcanic Stratospheric Sulfate Aerosol Forcing Emulator (EVA_H): Comparison With Interactive Stratospheric Aerosol Models. Journal of Geophysical Research-Atmospheres, 125(3). doi:10.1029/2019jd031303

Austin, W. E. N., Wilson, L. J., and Hunt, J. B.: The age and chronostratigraphical significance of North Atlantic Ash Zone II, Journal of Quaternary Science, 19, 137-146, 10.1002/jqs.821, 2004.

Baldini, J. U. L., Brown, R. J., and Mawdsley, N.: Evaluating the link between the sulfur-rich Laacher See volcanic eruption and the Younger Dryas climate anomaly, Climate of the Past, 14, 969-990, 10.5194/cp-14-969-2018, 2018.

Baroni, M., Savarino, J., Cole-Dai, J. H., Rai, V. K., and Thiemens, M. H.: Anomalous sulfur isotope compositions of volcanic sulfate over the last millennium in Antarctic ice cores, Journal of Geophysical Research-Atmospheres, 113, 10.1029/2008jd010185, 2008.

Bazin, L., Landais, A., Lemieux-Dudon, B., Kele, H. T. M., Veres, D., Parrenin, F., Martinerie, P., Ritz, C., Capron, E., Lipenkov, V., Loutre, M. F., Raynaud, D., Vinther, B., Svensson, A., Rasmussen, S. O., Severi, M., Blunier, T., Leuenberger, M., Fischer, H., Masson-Delmotte, V., Chappellaz, J., and Wolff, E.: An optimized multi-proxy, multi-site Antarctic ice and gas orbital chronology (AICC2012): 120-800 ka, Climate of the Past, 9, 1715-1731, 10.5194/cp-9-1715-2013, 2013.

Bigler, M., Svensson, A., Kettner, E., Vallelonga, P., Nielsen, M. E., and Steffensen, J. P.: Optimization of High-Resolution Continuous Flow Analysis for Transient Climate Signals in Ice Cores, Environmental Science & Technology, 45, 4483-4489, 10.1021/es200118j, 2011.

Bigler, M.: Hochauflösende Spurenstoffmessungen an polaren Eisbohrkernen: Glazio-chemische und klimatische Prozessstudien, 2004.Ph.D. dissertation, Physics Institute, University of Bern, Switzerland, 2004.

Bourne, A. J., Abbott, P. M., Albert, P. G., Cook, E., Pearce, N. J. G., Ponomareva, V., Svensson, A., and Davies, S. M.: Underestimated risks of recurrent long-range ash dispersal from northern Pacific Arc volcanoes, Scientific Reports, 6, 10.1038/srep29837, 2016.

Bourne, A. J., Cook, E., Abbott, P. M., Seierstad, I. K., Steffensen, J. P., Svensson, A., Fischer, H., Schupbach, S., and Davies, S. M.: A tephra lattice for Greenland and a reconstruction of volcanic events spanning 25-45 ka b2k, Quaternary Science Reviews, 118, 122-141, 10.1016/j.quascirev.2014.07.017, 2015.

Bowen, H. J. M. (1979), Environmental Chemistry of the Elements, 333 pp., Academic Press, London.

Brauer, A., Endres, C., and Negendank, J. F. W.: Lateglacial calendar year chronology based on annually laminated sediments from Lake Meerfelder Maar, Germany, Quaternary International, 61, 17-25, 10.1016/s1040-6182(99)00014-2, 1999.

Brown, S.K., Crosweller, H.S., Sparks, R.S.J., Cottrell. E, Deligne, N.I., Guerrero, N.O., Hobbs, L., Kiyosugi, K., Loughlin, S.C., Siebert, L., Takarada, S.: Characterisation of the Quaternary eruption record: analysis of the Large Magnitude Explosive Volcanic Eruptions (LaMEVE) database. J Appl. Volcanol. 3, 5, https://doi.org/10.1186/2191-5040-3-5, 2014.

Bryson, R.U., Bryson, R.A., Ruter, A.: A calibrated radiocarbon database of late Quaternary volcanic eruptions. eEarth Discuss. 1, 123–134, 10.5194/eed-1-123-2006 2006.

Buizert, C., Cuffey, K. M., Severinghaus, J. P., Baggenstos, D., Fudge, T. J., Steig, E. J., Markle, B. R., Winstrup, M., Rhodes, R. H., Brook, E. J., Sowers, T. A., Clow, G. D., Cheng, H., Edwards, R. L., Sigl, M.,

McConnell, J. R., and Taylor, K. C.: The WAIS Divide deep ice core WD2014 chronology - Part 1: Methane synchronization (68-31 kaBP) and the gas age-ice age difference, Climate of the Past, 11, 153-173, 10.5194/cp-11-153-2015, 2015.

Burke, A., Moore, K. A., Sigl, M., Nita, D. C., McConnell, J. R., and Adkins, J. F.: Stratospheric eruptions from tropical and extra-tropical volcanoes constrained using high-resolution sulfur isotopes in ice cores, Earth and Planetary Science Letters, 521, 113-119, 10.1016/j.epsl.2019.06.006, 2019.

Capron, E., Rasmussen, S. O., Popp, T. J., Erhardt, T., Fischer, H., Landais, A., Pedro, J. B., Vettoretti, G., Grinsted, A., Gkinis, V., Vaughn, B., Svensson, A., Vinther, B. M., and White, J. W. C.: The anatomy of past abrupt warmings recorded in Greenland ice, Nature Communications, 12, 10.1038/s41467-021-22241-w, 2021.

Castellano, E., Becagli, S., Jouzel, J., Migliori, A., Severi, M., Steffensen, J. P., Traversi, R., and Udisti, R.: Volcanic eruption frequency over the last 45 ky as recorded in Epica-Dome C ice core (East Antarctica) and its relationship with climatic changes, Global and Planetary Change, 42, 195-205, 10.1016/j.gloplacha.2003.11.007, 2004.

Clausen, H. B., Hammer, C. U., Hvidberg, C. S., DahlJensen, D., Steffensen, J. P., Kipfstuhl, J., and Legrand, M.: A comparison of the volcanic records over the past 4000 years from the Greenland Ice Core Project and Dye 3 Greenland Ice Cores, Journal of Geophysical Research-Oceans, 102, 26707-26723, 10.1029/97jc00587, 1997.

Cole-Dai, J., Ferris, D. G., Kennedy, J. A., Michael, S., and McConnell, J.: Comprehensive Record of Volcanic Eruptions in the Holocene (11,000 years) From the WAIS Divide, Antarctica Ice Core, Journal of Geophysical Research-Atmospheres, 126, 10.1029/2020JD032855, 2021.

Cole-Dai, J., Ferris, D., Lanciki, A., Savarino, J., Baroni, M., and Thiemens, M. H.: Cold decade (AD 1810-1819) caused by Tambora (1815) and another (1809) stratospheric volcanic eruption, Geophysical Research Letters, 36, 10.1029/2009gl040882, 2009.

Cooper, C. L., Swindles, G. T., Savov, I. P., Schmidt, A., and Bacon, K. L.: Evaluating the relationship between climate change and volcanism, Earth-Science Reviews, 177, 238-247, 10.1016/j.earscirev.2017.11.009, 2018.

Crick, L., Burke, A., Hutchison, W., Kohno, M., Moore, K., A., S., J., Doyle, E. A., Mahony, S., Kipfstuhl, S., Rae, J. W. B., and Steele, R. C. J., Sparks, R. S. J., and Wolff, E. W.: New insights into the ~74 ka Toba eruption from sulfur isotopes of polar ice cores, Clim. Past Discuss, https://doi.org/10.5194/cp-2021-38, in review, 2021, 2021.

Crowley, T. J. and Unterman, M. B.: Technical details concerning development of a 1200 yr proxy index for global volcanism, Earth System Science Data, 5, 187-197, 10.5194/essd-5-187-2013, 2013.

Dahl-Jensen, D., Albert, M. R., Aldahan, A., Azuma, N., Balslev-Clausen, D., Baumgartner, M., Berggren, A. M., Bigler, M., Binder, T., Blunier, T., Bourgeois, J. C., Brook, E. J., Buchardt, S. L., Buizert, C., Capron, E., Chappellaz, J., Chung, J., Clausen, H. B., Cvijanovic, I., Davies, S. M., Ditlevsen, P., Eicher, O., Fischer, H., Fisher, D. A., Fleet, L. G., Gfeller, G., Gkinis, V., Gogineni, S., Goto-Azuma, K., Grinsted, A., Gudlaugsdottir, H., Guillevic, M., Hansen, S. B., Hansson, M., Hirabayashi, M., Hong, S., Hur, S. D., Huybrechts, P., Hvidberg, C. S., Iizuka, Y., Jenk, T., Johnsen, S. J., Jones, T. R., Jouzel, J., Karlsson, N. B., Kawamura, K., Keegan, K., Kettner, E., Kipfstuhl, S., Kjaer, H. A., Koutnik, M., Kuramoto, T., Kohler, P., Laepple, T., Landais, A., Langen, P. L., Larsen, L. B., Leuenberger, D., Leuenberger, M., Leuschen, C., Li, J., Lipenkov, V., Martinerie, P., Maselli, O. J., Masson-Delmotte, V., McConnell, J. R., Miller, H., Mini, O., Miyamoto, A., Montagnat-Rentier, M., Mulvaney, R., Muscheler, R., Orsi, A. J., Paden, J., Panton, C., Pattyn, F., Petit, J. R., Pol, K., Popp, T., Possnert, G., Prie, F., Prokopiou, M., Quiquet, A., Rasmussen, S. O., Raynaud, D., Ren, J., Reutenauer, C., Ritz, C., Rockmann, T., Rosen, J. L., Rubino, M., Rybak, O., Samyn, D., Sapart, C. J., Schilt, A., Schmidt, A. M. Z., Schwander, J., Schupbach, S., Seierstad, I., Severinghaus, J. P., Sheldon, S., Simonsen, S. B., Sjolte, J., Solgaard, A. M., Sowers, T., Sperlich, P., Steen-Larsen, H. C., Steffen, K., Steffensen, J. P., Steinhage, D., Stocker, T. F., Stowasser, C., Sturevik, A. S., Sturges, W. T., Sveinbjornsdottir, A., Svensson, A., Tison, J. L., Uetake, J., Vallelonga, P., van de Wal, R. S. W., van der Wel, G., Vaughn, B. H., Vinther, B., Waddington, E., Wegner, A., Weikusat, I., White, J. W. C., Wilhelms, F., Winstrup, M., Witrant, E., Wolff, E. W., Xiao, C., Zheng, J., and Community, N.: Eemian interglacial reconstructed from a Greenland folded ice core, Nature, 493, 489-494, 10.1038/nature11789, 2013.

Dansgaard, W., Johnsen, S. J., Clausen, H. B., Dahljensen, D., Gundestrup, N. S., Hammer, C. U., Hvidberg, C. S., Steffensen, J. P., Sveinbjornsdottir, A. E., Jouzel, J., and Bond, G.: EVIDENCE FOR GENERAL INSTABILITY OF PAST CLIMATE FROM A 250-KYR ICE-CORE RECORD, Nature, 364, 218-220, 10.1038/364218a0, 1993.

Davies, S. M., Abbott, P. M., Pearce, N. J. G., Wastegard, S., and Blockley, S. P. E.: Integrating the INTIMATE records using tephrochronology: rising to the challenge, Quaternary Science Reviews, 36, 11-27, 10.1016/j.quascirev.2011.04.005, 2012.

Davies, S. M., Wastegard, S., Abbott, P. M., Barbante, C., Bigler, M., Johnsen, S. J., Rasmussen, T. L., Steffensen, J. P., and Svensson, A.: Tracing volcanic events in the NGRIP ice-core and synchronising North

Atlantic marine records during the last glacial period, Earth and Planetary Science Letters, 294, 69-79, 10.1016/j.epsl.2010.03.004, 2010.

Davies, S. M., Abbott, P. M., Meara, R. H., Pearce, N. J. G., Austin, W. E. N., Chapman, M. R., Svensson, A., Bigler, M., Rasmussen, T. L., Rasmussen, S. O., and Farmer, E. J.: A North Atlantic tephrostratigraphical framework for 130-60 ka b2k: new tephra discoveries, marine-based correlations, and future challenges, Quaternary Science Reviews, 106, 101-121, 10.1016/j.quascirev.2014.03.024, 2014.

Deligne, N. I., Coles, S. G., and Sparks, R. S. J.: Recurrence rates of large explosive volcanic eruptions, Journal of Geophysical Research-Solid Earth, 115, 10.1029/2009jb006554, 2010.

Dunbar, N. W., Iverson, N. A., Van Eaton, A. R., Sigl, M., Alloway, B. V., Kurbatov, A. V., Mastin, L. G., McConnell, J. R., and Wilson, C. J. N.: New Zealand supereruption provides time marker for the Last Glacial Maximum in Antarctica, Scientific Reports, 7, 10.1038/s41598-017-11758-0, 2017.

Eliza Cook, Siwan M. Davies, Peter M. Abbott, Nick J.G. Pearce, Seyedhamidreza Mojtabavi, Anders Svensson, Anna J. Bourne, Rhian H. Meara, Sune O. Rasmussen, Joseph Harrison, Elliott Street, Inger K. Seierstad, Bo M. Vinther, Jørgen Peder Steffensen, An updated record of volcanism in Greenland's ice between 12.1 and 17.4 ka b2k: A new tephrochronology framework based on cryptotephra deposits in three ice cores (in preparation).

Fischer, H., Wagenbach, D., and Kipfstuhl, J.: Sulfate and nitrate firn concentrations on the Greenland ice sheet - 2. Temporal anthropogenic deposition changes, Journal of Geophysical Research-Atmospheres, 103, 21935-21942, 10.1029/98jd01886, 1998.

Fudge, T. J., Markle, B. R., Cuffey, K. M., Buizert, C., Taylor, K. C., Steig, E. J., Waddington, E. D., Conway, H., and Koutnik, M.: Variable relationship between accumulation and temperature in West Antarctica for the past 31,000 years, Geophysical Research Letters, 43, 3795-3803, 10.1002/2016GL068356, 2016.

Fudge, T. J., Steig, E. J., Markle, B. R., Schoenemann, S. W., Ding, Q. H., Taylor, K. C., McConnell, J. R., Brook, E. J., Sowers, T., White, J. W. C., Alley, R. B., Cheng, H., Clow, G. D., Cole-Dai, J., Conway, H., Cuffey, K. M., Edwards, J. S., Edwards, R. L., Edwards, R., Fegyveresi, J. M., Ferris, D., Fitzpatrick, J. J., Johnson, J., Hargreaves, G., Lee, J. E., Maselli, O. J., Mason, W., McGwire, K. C., Mitchell, L. E., Mortensen, N., Neff, P., Orsi, A. J., Popp, T. J., Schauer, A. J., Severinghaus, J. P., Sigl, M., Spencer, M. K., Vaughn, B. H., Voigt, D. E., Waddington, E. D., Wang, X. F., Wong, G. J., and Members, W. D. P.: Onset of deglacial warming in West Antarctica driven by local orbital forcing, Nature, 500, 440-+, 10.1038/nature12376, 2013.

Gao, C. C., Robock, A., and Ammann, C.: Volcanic forcing of climate over the past 1500 years: An improved ice core-based index for climate models, Journal of Geophysical Research-Atmospheres, 113, 10.1029/2008jd010239, 2008.

Gao, C. H., Oman, L., Robock, A., and Stenchikov, G. L.: Atmospheric volcanic loading derived from bipolar ice cores: Accounting for the spatial distribution of volcanic deposition, Journal of Geophysical Research-Atmospheres, 112, 10.1029/2006jd007461, 2007.

Gautier, E., Savarino, J., Erbland, J., and Farquhar, J.: SO2 Oxidation Kinetics Leave a Consistent Isotopic Imprint on Volcanic Ice Core Sulfate, Journal of Geophysical Research-Atmospheres, 123, 9801-9812, 10.1029/2018jd028456, 2018.

Gautier, E., Savarino, J., Erbland, J., Lanciki, A., and Possenti, P.: Variability of sulfate signal in ice core records based on five replicate cores, Climate of the Past, 12, 103-113, 10.5194/cp-12-103-2016, 2016.

Giaccio, B., Hajdas, I., Isaia, R., Deino, A., and Nomade, S.: High-precision C-14 and Ar-40/Ar-39 dating of the Campanian Ignimbrite (Y-5) reconciles the time-scales of climatic-cultural processes at 40 ka, Scientific Reports, 7, 10.1038/srep45940, 2017.

Gronvold, K., Oskarsson, N., Johnsen, S. J., Clausen, H. B., Hammer, C. U., Bond, G., and Bard, E.: ASH LAYERS FROM ICELAND IN THE GREENLAND GRIP ICE CORE CORRELATED WITH OCEANIC AND LAND SEDIMENTS, Earth and Planetary Science Letters, 135, 149-155, 10.1016/0012-821x(95)00145-3, 1995.

Grootes, P. M., Stuiver, M., White, J. W. C., Johnsen, S., and Jouzel, J.: COMPARISON OF OXYGEN-ISOTOPE RECORDS FROM THE GISP2 AND GRIP GREENLAND ICE CORES, Nature, 366, 552-554, 10.1038/366552a0, 1993.

Hansen, J., Sato, M., Ruedy, R., Nazarenko, L., Lacis, A., Schmidt, G. A., Russell, G., Aleinov, I., Bauer, M., Bauer, S., Bell, N., Cairns, B., Canuto, V., Chandler, M., Cheng, Y., Genio, A. Del, Faluvegi, G., Fleming, E., Friend, A., Hall, T., Jackman, C., Kelley, M., Kiang, N., Koch, D., Lean, J., Lerner, J., Lo, K., Menon, S., Miller, R., Minnis, P., Novakov, T., Oinas, V., Perlwitz, J., Perlwitz, J., Rind, D., Romanou, A., Shindell, D., Stone, P., Sun, S., Tausnev, N., Thresher, D., Wielicki, B., Wong, T., Yao, M., Zhang, S.: Efficacy of climate forcings, Journal of Geophysical Research 110(D18), D18104, 2005.

Herweijer, C., Seager, R., Cook, E. R., and Emile-Geay, J.: North American droughts of the last millennium from a gridded network of tree-ring data, Journal of Climate, 20, 1353-1376, 10.1175/jcli4042.1, 2007.

Huybers, P. and Langmuir, C.: Feedback between deglaciation, volcanism, and atmospheric CO2, Earth and Planetary Science Letters, 286, 479-491, 10.1016/j.epsl.2009.07.014, 2009.

Hvidberg, C. S., DahlJensen, D., and Waddington, E. D.: Ice flow between the Greenland Ice Core Project and Greenland Ice Sheet Project 2 boreholes in central Greenland, Journal of Geophysical Research-Oceans, 102, 26851-26859, 10.1029/97jc00268, 1997.

Johnsen, S. J., DahlJensen, D., Gundestrup, N., Steffensen, J. P., Clausen, H. B., Miller, H., . . . White, J. (2001). Oxygen isotope and palaeotemperature records from six Greenland ice-core stations: Camp Century, Dye-3, GRIP, GISP2, Renland and NorthGRIP. *Journal of Quaternary Science*, *16*(4), 299-307. doi:10.1002/jqs.622

Jungclaus, J. H., Bard, E., Baroni, M., Braconnot, P., Cao, J., Chini, L. P., Egorova, T., Evans, M., Gonzalez-Rouco, J. F., Goosse, H., Hurtt, G. C., Joos, F., Kaplan, J. O., Khodri, M., Goldewijk, K. K., Krivova, N., LeGrande, A. N., Lorenz, S. J., Luterbacher, J., Man, W. M., Maycock, A. C., Meinshausen, M., Moberg, A., Muscheler, R., Nehrbass-Ahles, C., Otto-Bliesner, B. I., Phipps, S. J., Pongratz, J., Rozanov, E., Schmidt, G. A., Schmidt, H., Schmutz, W., Schurer, A., Shapiro, A. I., Sigl, M., Smerdon, J. E., Solanki, S. K., Timmreck, C., Toohey, M., Usoskin, I. G., Wagner, S., Wu, C. J., Yeo, K. L., Zanchettin, D., Zhang, Q., and Zorita, E.: The PMIP4 contribution to CMIP6-Part 3: The last millennium, scientific objective, and experimental design for the PMIP4 past1000 simulations, Geoscientific Model Development, 10, 4005-4033, 10.5194/gmd-10-4005-2017, 2017.

Karlof, L., Oigard, T. A., Godtliebsen, F., Kaczmarska, M., and Fischer, H.: Statistical techniques to select detection thresholds for peak signals in ice-core data, Journal of Glaciology, 51, 655-662, 10.3189/172756505781829115, 2005.

Kreutz, K. J., Mayewski, P. A., Meeker, L. D., Twickler, M. S., and Whitlow, S. I.: The effect of spatial and temporal accumulation rate variability in West Antarctica on soluble ion deposition, Geophysical Research Letters, 27, 2517-2520, 10.1029/2000gl011499, 2000.

Kurbatov, A. V., Zielinski, G. A., Dunbar, N. W., Mayewski, P. A., Meyerson, E. A., Sneed, S. B., and Taylor, K. C.: A 12,000 year record of explosive volcanism in the Siple Dome Ice Core, West Antarctica, Journal of Geophysical Research-Atmospheres, 111, 10.1029/2005jd006072, 2006.

Kutterolf, S., Schindlbeck, J. C., Jegen, M., Freundt, A., and Straub, S. M.: Milankovitch frequencies in tephra records at volcanic arcs: The relation of kyr-scale cyclic variations in volcanism to global climate changes, Quaternary Science Reviews, 204, 1-16, 10.1016/j.quascirev.2018.11.004, 2019.

Lane, C. S., Blockley, S. P. E., Mangerud, J., Smith, V. C., Lohne, O. S., Tomlinson, E. L., Matthews, I. P., and Lotter, A. F.: Was the 12.1 ka Icelandic Vedde Ash one of a kind?, Quaternary Science Reviews, 33, 87-99, 10.1016/j.quascirev.2011.11.011, 2012.

Legrand, M. and Mayewski, P.: Glaciochemistry of polar ice cores: A review, Reviews of Geophysics, 35, 219-243, 10.1029/96rg03527, 1997.

Legrand, M., Hammer, C., DeAngelis, M., Savarino, J., Delmas, R., Clausen, H., and Johnsen, S. J.: Sulfur-containing species (methanesulfonate and SO4) over the last climatic cycle in the Greenland Ice Core Project (central Greenland) ice core, Journal of Geophysical Research-Oceans, 102, 26663-26679, 10.1029/97jc01436, 1997.

Lim, H. G., Yeh, S. W., Kug, J. S., Park, Y. G., Park, J. H., Park, R., and Song, C. K.: Threshold of the volcanic forcing that leads the El Nino-like warming in the last millennium: results from the ERIK simulation, Climate Dynamics, 46, 3725-3736, 10.1007/s00382-015-2799-3, 2016.

Maclennan, J., Jull, M., McKenzie, D., Slater, L., and Gronvold, K.: The link between volcanism and deglaciation in Iceland, Geochemistry Geophysics Geosystems, 3, 10.1029/2001gc000282, 2002.

Marshall, L., Johnson, J. S., Mann, G. W., Lee, L., Dhomse, S. S., Regayre, L., . . . Schmidt, A. (2019). Exploring How Eruption Source Parameters Affect Volcanic Radiative Forcing Using Statistical Emulation. Journal of Geophysical Research-Atmospheres, 124(2), 964-985. doi:10.1029/2018jd028675

Marshall, L. R., Smith, C. J., Forster, P. M., Aubry, T. J., Andrews, T., & Schmidt, A. (2020). Large Variations in Volcanic Aerosol Forcing Efficiency Due to Eruption Source Parameters and Rapid Adjustments. Geophysical Research Letters, 47(19). doi:10.1029/2020gl090241

Mayewski, P. A., Holdsworth, G., Spencer, M. J., Whitlow, S., Twickler, M., Morrison, M. C., Ferland, K. K., and Meeker, L. D.: ICE-CORE SULFATE FROM 3 NORTHERN-HEMISPHERE SITES - SOURCE AND TEMPERATURE FORCING IMPLICATIONS, Atmospheric Environment Part a-General Topics, 27, 2915-2919, 10.1016/0960-1686(93)90323-q, 1993.

Mayewski, P. A., Meeker, L. D., Twickler, M. S., Whitlow, S., Yang, Q. Z., Lyons, W. B., and Prentice, M.: Major features and forcing of high-latitude northern hemisphere atmospheric circulation using a 110,000-year-long glaciochemical series, Journal of Geophysical Research-Oceans, 102, 26345-26366, 10.1029/96jc03365, 1997.

McConnell, J. R., Burke, A., Dunbar, N. W., Kohler, P., Thomas, J. L., Arienzo, M. M., Chellman, N. J., Maselli, O. J., Sigl, M., Adkins, J. F., Baggenstos, D., Burkhart, J. F., Brook, E. J., Buizert, C., Cole-Dai, J., Fudge, T. J., Knorr, G., Graf, H. F., Grieman, M. M., Iverson, N., McGwire, K. C., Mulvaney, R., Paris, G., Rhodes, R. H., Saltzman, E. S., Severinghaus, J. P., Steffensen, J. P., Taylor, K. C., and Winckler, G.: Synchronous volcanic eruptions and abrupt climate change similar to 17.7 ka plausibly linked by

stratospheric ozone depletion, Proceedings of the National Academy of Sciences of the United States of America, 114, 10035-10040, 10.1073/pnas.1705595114, 2017.

Mortensen, A. K., Bigler, M., Gronvold, K., Steffensen, J. P., and Johnsen, S. J.: Volcanic ash layers from the Last Glacial Termination in the NGRIP ice core, Journal of Quaternary Science, 20, 209-219, 10.1002/jqs.908, 2005.

Narcisi, B., Petit, J. R., and Chappellaz, J.: A 70 ka record of explosive eruptions from the TALDICE ice core (Talos Dome, East Antarctic plateau), Journal of Quaternary Science, 25, 844-849, 10.1002/jqs.1427, 2010.

Narcisi, B., Petit, J. R., Delmonte, B., Basile-Doelsch, I., and Maggi, V.: Characteristics and sources of tephra layers in the EPICA-Dome C ice record (East Antarctica): Implications for past atmospheric circulation and ice core stratigraphic correlations, Earth and Planetary Science Letters, 239, 253-265, 10.1016/j.epsl.2005.09.005, 2005.

Narcisi, B., Petit, J. R., Delmonte, B., Scarchilli, C., and Stenni, B.: A 16,000-yr tephra framework for the Antarctic ice sheet: a contribution from the new Tabs Dome core, Quaternary Science Reviews, 49, 52-63, 10.1016/j.quascirev.2012.06.011, 2012.

Nardin, R., Amore, A., Becagli, S., Caiazzo, L., Frezzotti, M., Severi, M., Stenni, B., and Traversi, R.: Volcanic Fluxes Over the Last Millennium as Recorded in the Gv7 Ice Core (Northern Victoria Land, Antarctica), Geosciences, 10, 10.3390/geosciences10010038, 2020.

Nordhausen, K. The Elements of Statistical Learning: Data Mining, Inference, and Prediction, Second Edition by Trevor Hastie, Robert Tibshirani, Jerome Friedman; Springer: New York, NY, USA, 2009; pp. 37–38. doi:10.1111/j.1751-5823.2009.00095_18.x

Parrenin, F., Petit, J. R., Masson-Delmotte, V., Wolff, E., Basile-Doelsch, I., Jouzel, J., Lipenkov, V., Rasmussen, S. O., Schwander, J., Severi, M., Udisti, R., Veres, D., and Vinther, B. M.: Volcanic synchronisation between the EPICA Dome C and Vostok ice cores (Antarctica) 0-145 kyr BP, Climate of the Past, 8, 1031-1045, 10.5194/cp-8-1031-2012, 2012.

Papale, P.: Global time-size distribution of volcanic eruptions on Earth, Scientific Reports, 8, 10.1038/s41598-018-25286-y, 2018.

Plummer, C. T., Curran, M. A. J., van Ommen, T. D., Rasmussen, S. O., Moy, A. D., Vance, T. R., Clausen, H. B., Vinther, B. M., and Mayewski, P. A.: An independently dated 2000-yr volcanic record from Law Dome, East Antarctica, including a new perspective on the dating of the 1450s CE eruption of Kuwae, Vanuatu, Climate of the Past, 8, 1929-1940, 10.5194/cp-8-1929-2012, 2012.

Praetorius, S., Mix, A., Jensen, B., Froese, D., Milne, G., Wolhowe, M., Addison, J., and Prahl, F.: Interaction between climate, volcanism, and isostatic rebound in Southeast Alaska during the last deglaciation, Earth and Planetary Science Letters, 452, 79-89, 10.1016/j.epsl.2016.07.033, 2016.

Pyle, D. M.: Chapter 13 - Sizes of Volcanic Eruptions. In: The Encyclopedia of Volcanoes (Second Edition), Sigurdsson, H. (Ed.), Academic Press, Amsterdam, 2015.

Rasmussen, S. O., Abbott, P. M., Blunier, T., Bourne, A. J., Brook, E., Buchardt, S. L., Buizert, C., Chappellaz, J., Clausen, H. B., Cook, E., Dahl-Jensen, D., Davies, S. M., Guillevic, M., Kipfstuhl, S., Laepple, T., Seierstad, I. K., Severinghaus, J. P., Steffensen, J. P., Stowasser, C., Svensson, A., Vallelonga, P., Vinther, B. M., Wilhelms, F., and Winstrup, M.: A first chronology for the North Greenland Eemian Ice Drilling (NEEM) ice core, Climate of the Past, 9, 2713-2730, 10.5194/cp-9-2713-2013, 2013.

Rasmussen, S. O., Andersen, K. K., Johnsen, S. J., Bigler, M., and McCormack, T.: Deconvolution-based resolution enhancement of chemical ice core records obtained by continuous flow analysis, Journal of Geophysical Research-Atmospheres, 110, 10.1029/2004jd005717, 2005.

Rasmussen, S. O., Bigler, M., Blockley, S. P., Blunier, T., Buchardt, S. L., Clausen, H. B., Cvijanovic, I., Dahl-Jensen, D., Johnsen, S. J., Fischer, H., Gkinis, V., Guillevic, M., Hoek, W. Z., Lowe, J. J., Pedro, J. B., Popp, T., Seierstad, I. K., Steffensen, J. P., Svensson, A. M., Vallelonga, P., Vinther, B. M., Walker, M. J. C., Wheatley, J. J., and Winstrup, M.: A stratigraphic framework for abrupt climatic changes during the Last Glacial period based on three synchronized Greenland ice-core records: refining and extending the INTIMATE event stratigraphy, Quaternary Science Reviews, 106, 14-28, 10.1016/j.quascirev.2014.09.007, 2014.

Reinig, F. et al.: Precise date for the Laacher See eruption synchronizes the Younger Dryas, Nature, 595, 66–69, 2021.

Robock, A.: Volcanic eruptions and climate, Reviews of Geophysics, 38, 191-219, 10.1029/1998rg000054, 2000.

Rutledal, S., Berben, S. M. P., Dokken, T. M., van der Bilt, W. G. M., Cederstrom, J. M., and Jansen, E.: Tephra horizons identified in the western North Atlantic and Nordic Seas during the Last Glacial Period: Extending the marine tephra framework, Quaternary Science Reviews, 240, 10.1016/j.quascirev.2020.106247, 2020.

Ruth, U., Barnola, J. M., Beer, J., Bigler, M., Blunier, T., Castellano, E., Fischer, H., Fundel, F., Huybrechts, P., Kaufmann, P., Kipfstuhl, S., Lambrecht, A., Morganti, A., Oerter, H., Parrenin, F., Rybak, O., Severi, M., Udisti, R., Wilhelms, F., and Wolff, E.: "EDML1": a chronology for the EPICA deep ice core from Dronning

Maud Land, Antarctica, over the last 150 000 years, Climate of the Past, 3, 475-484, 10.5194/cp-3-475-2007, 2007.

Ruth, U., Wagenbach, D., Steffensen, J. P., and Bigler, M.: Continuous record of microparticle concentration and size distribution in the central Greenland NGRIP ice core during the last glacial period, Journal of Geophysical Research-Atmospheres, 108, 10.1029/2002jd002376, 2003.

Röthlisberger, R., Bigler, M., Hutterli, M., Sommer, S., Stauffer, B., Junghans, H. G., and Wagenbach, D.: Technique for continuous high-resolution analysis of trace substances in firn and ice cores, Environmental Science & Technology, 34, 338-342, 2000.

Sinnl, G., Winstrup, M., Erhardt, T., Cook, E., Jensen, C., Svensson, A., Vinther, B. M., Muscheler, R., and Rasmussen, S. O.: A multi-ice-core, annual-layer-counted Greenland ice-core chronology for the last 3800 years: GICC21, Clim. Past Discuss. [preprint], https://doi.org/10.5194/cp-2021-155, in review, 2021.

Schupbach, S., Fischer, H., Bigler, M., Erhardt, T., Gfeller, G., Leuenberger, D., Mini, O., Mulvaney, R., Abram, N. J., Fleet, L., Frey, M. M., Thomas, E., Svensson, A., Dahl-Jensen, D., Kettner, E., Kjaer, H., Seierstad, I., Steffensen, J. P., Rasmussen, S. O., Vallelonga, P., Winstrup, M., Wegner, A., Twarloh, B., Wolff, K., Schmidt, K., Goto-Azuma, K., Kuramoto, T., Hirabayashi, M., Uetake, J., Zheng, J., Bourgeois, J., Fisher, D., Zhiheng, D., Xiao, C., Legrand, M., Spolaor, A., Gabrieli, J., Barbante, C., Kang, J. H., Hur, S. D., Hong, S. B., Hwang, H. J., Hong, S., Hansson, M., Iizuka, Y., Oyabu, I., Muscheler, R., Adolphi, F., Maselli, O., McConnell, J., and Wolff, E. W.: Greenland records of aerosol source and atmospheric lifetime changes from the Eemian to the Holocene, Nature Communications, 9, 10.1038/s41467-018-03924-3, 2018.

Schurer, A. P., Tett, S. F. B., and Hegerl, G. C.: Small influence of solar variability on climate over the past millennium, Nature Geoscience, 7, 104-108, 10.1038/ngeo2040, 2014.

Seierstad, I. K., Abbott, P. M., Bigler, M., Blunier, T., Bourne, A. J., Brook, E., Buchardt, S. L., Buizert, C., Clausen, H. B., Cook, E., Dahl-Jensen, D., Davies, S. M., Guillevic, M., Johnsen, S. J., Pedersen, D. S., Popp, T. J., Rasmussen, S. O., Severinghaus, J. P., Svensson, A., and Vinther, B. M.: Consistently dated records from the Greenland GRIP, GISP2 and NGRIP ice cores for the past 104 ka reveal regional millennial-scale delta O-18 gradients with possible Heinrich event imprint, Quaternary Science Reviews, 106, 29-46, 10.1016/j.quascirev.2014.10.032, 2014.

Severi, M., Becagli, S., Castellano, E., Morganti, A., Traversi, R., Udisti, R., Ruth, U., Fischer, H., Huybrechts, P., Wolff, E., Parrenin, F., Kaufmann, P., Lambert, F., and Steffensen, J. P.: Synchronisation of the EDML

and EDC ice cores for the last 52 kyr by volcanic signature matching, Climate of the Past, 3, 367-374, 10.5194/cp-3-367-2007, 2007.

Severi, M., Becagli, S., Traversi, R., and Udisti, R.: Recovering Paleo-Records from Antarctic Ice-Cores by Coupling a Continuous Melting Device and Fast Ion Chromatography, Analytical Chemistry, 87, 11441-11447, 10.1021/acs.analchem.5b02961, 2015.

Siebert, L., Simkin, T.: Volcanoes of the world: an illustrated catalog of Holocene volcanoes and their eruptions. Smithsonian Institution, Global Volcanism Program, Digital Information Series. GVP-3, 2002.

Sigl, M., McConnell, J. R., Layman, L., Maselli, O., McGwire, K., Pasteris, D., Dahl-Jensen, D., Steffensen, J. P., Vinther, B., Edwards, R., Mulvaney, R., and Kipfstuhl, S.: A new bipolar ice core record of volcanism from WAIS Divide and NEEM and implications for climate forcing of the last 2000 years, Journal of Geophysical Research-Atmospheres, 118, 1151-1169, 10.1029/2012jd018603, 2013.

Sigl, M., McConnell, J. R., Toohey, M., Curran, M., Das, S. B., Edwards, R., Isaksson, E., Kawamura, K., Kipfstuhl, S., Kruger, K., Layman, L., Maselli, O. J., Motizuki, Y., Motoyama, H., Pasteris, D. R., and Severi, M.: Insights from Antarctica on volcanic forcing during the Common Era, Nature Climate Change, 4, 693-697, 10.1038/nclimate2293, 2014.

Sigl, M., Winstrup, M., McConnell, J. R., Welten, K. C., Plunkett, G., Ludlow, F., Buntgen, U., Caffee, M., Chellman, N., Dahl-Jensen, D., Fischer, H., Kipfstuhl, S., Kostick, C., Maselli, O. J., Mekhaldi, F., Mulvaney, R., Muscheler, R., Pasteris, D. R., Pilcher, J. R., Salzer, M., Schupbach, S., Steffensen, J. P., Vinther, B. M., and Woodruff, T. E.: Timing and climate forcing of volcanic eruptions for the past 2,500 years, Nature, 523, 543-+, 10.1038/nature14565, 2015.

Sigl, M., Fudge, T. J., Winstrup, M., Cole-Dai, J., Ferris, D., McConnell, J. R., Taylor, K. C., Welten, K. C., Woodruff, T. E., Adolphi, F., Bisiaux, M., Brook, E. J., Buizert, C., Caffee, M. W., Dunbar, N. W., Edwards, R., Geng, L., Iverson, N., Koffman, B., Layman, L., Maselli, O. J., McGwire, K., Muscheler, R., Nishiizumi, K., Pasteris, D. R., Rhodes, R. H., and Sowers, T. A.: The WAIS Divide deep ice core WD2014 chronology - Part 2: Annual-layer counting (0-31 ka BP), Clim. Past., 12, 769-786, 10.5194/cp-12-769-2016, 2016.

Siggaard-Andersen, M. L. (2004): Analysis of soluble ions from dust and sea salt over the last glacial cycle in polar deep ice cores , PhD thesis, University of Bremen.

Svensson, A., Biscaye, P. E., and Grousset, F. E.: Characterization of late glacial continental dust in the Greenland Ice Core Project ice core, Journal of Geophysical Research-Atmospheres, 105, 4637-4656, 10.1029/1999jd901093, 2000.

Svensson, A., Dahl-Jensen, D., Steffensen, J. P., Blunier, T., Rasmussen, S. O., Vinther, B. M., Vallelonga, P., Capron, E., Gkinis, V., Cook, E., Kjaer, H. A., Muscheler, R., Kipfstuhl, S., Wilhelms, F., Stocker, T. F., Fischer, H., Adolphi, F., Erhardt, T., Sigl, M., Landais, A., Parrenin, F., Buizert, C., McConnell, J. R., Severi, M., Mulvaney, R., and Bigler, M.: Bipolar volcanic synchronization of abrupt climate change in Greenland and Antarctic ice cores during the last glacial period, Climate of the Past, 16, 1565-1580, 10.5194/cp-16-1565-2020, 2020.

Taylor, K. C., Alley, R. B., Lamorey, G. W., and Mayewski, P.: Electrical measurements on the Greenland Ice Sheet Project 2 core, Journal of Geophysical Research-Oceans, 102, 26511-26517, 10.1029/96jc02500, 1997.

Timmreck, C., Pohlmann, H., Illing, S., and Kadow, C.: The impact of stratospheric volcanic aerosol on decadal-scale climate predictions, Geophysical Research Letters, 43, 834-842, 10.1002/2015gl067431, 2016.

Toohey, M. and Sigl, M.: Volcanic stratospheric sulfur injections and aerosol optical depth from 500 BCE to 1900 CE, Earth System Science Data, 9, 809-831, 10.5194/essd-9-809-2017, 2017.

Toohey, M., Kruger, K., Schmidt, H., Timmreck, C., Sigl, M., Stoffel, M., and Wilson, R.: Disproportionately strong climate forcing from extratropical explosive volcanic eruptions, Nature Geoscience, 12, 100-+, 10.1038/s41561-018-0286-2, 2019.

Van Vliet-Lanoe, B., Bergerat, F., Allemand, P., Innocentd, C., Guillou, H., Cavailhes, T., Gudmundsson, A., Chazot, G., Schneider, J. L., Grandjean, P., Liorzou, C., and Passot, S.: Tectonism and volcanism enhanced by deglaciation events in southern Iceland, Quaternary Research, 94, 94-120, 10.1017/qua.2019.68, 2020.

Vapnik V. (1998) The Support Vector Method of Function Estimation. In: Suykens J.A.K., Vandewalle J. (eds) Nonlinear Modeling. Springer, Boston, MA. https://doi.org/10.1007/978-1-4615-5703-6_3

Veres, D., Bazin, L., Landais, A., Kele, H. T. M., Lemieux-Dudon, B., Parrenin, F., Martinerie, P., Blayo, E., Blunier, T., Capron, E., Chappellaz, J., Rasmussen, S. O., Severi, M., Svensson, A., Vinther, B., and Wolff, E. W.: The Antarctic ice core chronology (AICC2012): an optimized multi-parameter and multi-site dating approach for the last 120 thousand years, Climate of the Past, 9, 1733-1748, 10.5194/cp-9-1733-2013, 2013.

Watt, S. F. L., Pyle, D. M., and Mather, T. A.: The volcanic response to deglaciation: Evidence from glaciated arcs and a reassessment of global eruption records, Earth-Science Reviews, 122, 77-102, 10.1016/j.earscirev.2013.03.007, 2013.

Zielinski, G. A., Mayewski, P. A., Meeker, L. D., Whitlow, S., and Twickler, M. S.: A 110,000-yr record of explosive volcanism from the GISP2 (Greenland) ice core, Quaternary Research, 45, 109-118, 10.1006/qres.1996.0013, 1996.

Zielinski, G. A., Mayewski, P. A., Meeker, L. D., Gronvold, K., Germani, M. S., Whitlow, S., Twickler, M. S., and Taylor, K.: Volcanic aerosol records and tephrochronology of the Summit, Greenland, ice cores, Journal of Geophysical Research-Oceans, 102, 26625-26640, 10.1029/96jc03547, 1997.

Figure and table captions:

Table 1

The number and frequency of large bipolar volcanic eruptions for the last 2500 years and for the last glacial and early Holocene (this study). The climate forcing is calculated using the SAOD scaling of Aubry et al. (2020) and the radiative forcing conversion from Marshall et al. (2020).

Table 2

The largest bipolar volcanic eruptions of the last glacial period and early Holocene ranked by the volcanic aerosol forcing that is derived from the average Greenland and Antarctic volcanic sulfate depositions. The stratospheric aerosol loading was estimated according to Gao et al. (2007) and the radiative volcanic aerosol forcing was reconstructed with a scaling factor of SAOD obtained from Aubry et al. (2020) and a scaling factor to obtain the radiative forcing following Marshall et al. (2020) (section 4.3). 'NHHL' refers to high-latitude northern-hemisphere locations of volcanoes, meaning above 40° N; 'LL or SH' refers to low latitude or southern hemisphere locations, meaning below 40° N. 'Number of ice cores' refers to the number of ice cores in Greenland and Antarctica in which the volcanic sulfate signal has been detected.

Figure 1

Relationship between Greenland and Antarctic volcanic sulfate deposition for the large bipolar volcanic eruptions. The size of the circle relates to the stratospheric sulfate aerosol loading. (a) Volcanoes in the last glacial period are classified by a Support Vector Machine (SVM) model with latitudinal bands: above 40°N in red circles, below 40°N in blue circles. (b) Volcanoes of the last 2500 years for which the eruption site is known (listed in Table S6) are classified with the latitudinal bands as for (a).

Figure 2

The average volcanic sulfate deposition in Greenland and Antarctica (60-9 ka; 2.5-0 ka adapted from Sigl et al., 2013, 2015). The blue curve shows $\delta^{18}O$ of the NGRIP core. Greenland volcanic sulfate depositions larger than 20 kg km^{-2} (cyan bars) and Antarctic volcanic sulfate deposition larger than 10 kg km^{-2} (black bars) are shown. Bipolar volcanic eruptions are indicated with an 'x'.

Figure 3

Number (top) and volcanic sulfate deposition (bottom) of volcanoes per millennium detected in Greenland and Antarctic ice-core sulfate records with relatively similar data resolution for the last 2500 years and the late glacial period. Positive values represent Greenland volcanoes and negative values represent Antarctic volcanoes. The volcanic eruptions are grouped into three size fractions based on the 0.7 and 0.9 quantiles of the volcanic sulfate deposition distribution. For Greenland the classes are separated at 68 kg km^{-2} and 140 kg km^{-2} and for Antarctica the separation is made at 25 kg km^{-2} and 50 kg km^{-2}. The magnitude of volcanoes is represented by the average volcanic sulfate deposition in Greenland or in Antarctica. The records used for the figure as follows: For the last 2000 years (911-1911 AD and 89-911 AD), the volcanic sulfate deposition is based on the NEEM S1 and NGRIP cores for Greenland and on the WDC core for Antarctica (Sigl et al. 2013) using smoothed 2-year resolution sulfate records. For the period 60-9 ka the Greenland sulfate deposition is derived from NEEM, GISP2 and NGRIP. For GISP2, the data was smoothed to 5 years in the period of 14-9 ka and for the period older than 14 ka only large volcanic sulfate signals are detected. The NGRIP sulfate record has been smoothed to 2-year resolution throughout. For the period 60-9 ka the Antarctic sulfate deposition is derived from EDML, EDC and WDC sulfate records. The WDC sulfate record has been smoothed to 2-year resolution.

Figure 4

Comparison of the number of volcanic eruptions per millennium detected in Greenland and Antarctic ice cores grouped for different climatic periods with relatively similar data resolution for the last 2500 years and the late glacial period. The applied datasets and smoothing are the same as used for Fig. 3. The detected eruptions are classified into three size fractions similar to the approach of Fig. 3.

Figure 5

Cumulative number and sulfate deposition of volcanoes with time (same as in Fig. 2 and Tables S3 and S4) for three classified size fractions (same fractions as in Fig. 3) of volcanoes for Greenland and Antarctica (60-9 ka).

Figure 6

Schematic of the latitudinal location for the identified bipolar volcanic eruptions (Table S5). Volcanoes that erupted sites are predict above 40°N are marked at 40°N and those are predict below 40°N are marked at

Equator. Volcanic locations are known from ice-core tephra deposits that are indicated by name and age of the eruption (Table S5). The eruption at 38.1 ka is very likely from Southern Hemisphere but the erupted site is unknown. The size of the circles represents the strength of volcanic stratospheric aerosol loading.

Table 1

	Absolute number of eruptions		Eruptions per millennium	
	0-2.5 ka	9-16.5 ka 24.5-60 ka	0-2.5 ka	9-16.5 ka 24.5-60 ka
< -13.2 W m^{-2} (Oruanui, Taupo)	0	3	0	0.07
< -9.5 W m^{-2} (EU 426 BC)	1	25	0.4	0.58
< -6.5 W m^{-2} (Tambora)	6	69	2.4	1.60

1135

Table 2

Rank	Age (b2k)	Greenland volc. depo. (kg/km^2)	Antarctic volc. depo. (kg/km^2)	Stratospheric aerosol loading (Tg)	Global climate forcing (W/m^2)	Prediction of volcanic site	Number of ice cores	
							Greenland	Antarctica
1	55383	1117.4	16.5	653.4	-15.9	NHHL	3	2
2	45555	652.6	172.7	544.7	-15.0	NHHL	3	3
3	38133	209.4	204.5	413.9	-13.6	LL or SH	3	2
4	25460	189.5	192.8	382.3	-13.2	LL or SH	2	3
5	52302	293.0	185.4	352.4	-12.8	NHHL	3	3
6	44763	169.7	171.0	340.7	-12.7	LL or SH	2	3
7	29680	333.3	137.6	327.5	-12.5	NHHL	2	3
8	46683	105.1	211.1	316.2	-12.3	LL or SH	2	3
9	41144	410.0	81.8	315.5	-12.3	NHHL	3	3
10	49065	164.9	142.3	307.2	-12.1	LL or SH	3	3
11	42037	327.7	119.8	306.6	-12.1	NHHL	2	3
12	32032	210.8	145.6	265.8	-11.4	NHHL	3	3
13	25759	214.8	110.6	233.1	-10.8	NHHL	3	3
14	39915	316.0	44.0	224.1	-10.6	NHHL	3	3
15	34718	301.0	52.5	224.1	-10.6	NHHL	2	3
16	13028	272.8	65.0	220.5	-10.5	NHHL	3	3
17	12917	248.1	59.4	200.8	-10.0	NHHL	3	3
18	11305	297.8	30.1	199.8	-10.2	NHHL	2	3
19	47023	255.4	52.3	197.9	-10.0	NHHL	3	3
20	16469	102.9	89.8	192.7	-9.9	LL or SH	2	3
21	14761	307.8	10.7	186.2	-9.7	NHHL	3	3
22	28942	88.4	97.5	185.9	-9.7	LL or SH	1	3
23	42250	183.0	80.9	185.2	-9.7	NHHL	2	3
24	35556	236.4	45.4	180.1	-9.5	NHHL	3	3
25	44507	98.6	80.3	178.9	-9.5	LL or SH	1	2
26	40183	211.5	47.5	168.1	-9.2	NHHL	3	3
27	58182	156.9	78.6	168.1	-9.2	NHHL	1	3
28	27797	263.9	17.6	168.0	-9.2	NHHL	2	3
29	46116	66.5	99.4	165.9	-9.2	LL or SH	3	3
30	42658	133.1	85.6	161.5	-9.0	NHHL	3	3
31	24669	172.9	62.1	160.7	-9.0	NHHL	3	3
32	15559	84.0	72.2	156.2	-8.9	LL or SH	2	3
33	30244	208.7	36.3	155.2	-8.9	NHHL	3	2
34	29722	206.1	36.8	154.3	-8.8	NHHL	2	2
35	10481	170.6	56.7	153.9	-8.8	NHHL	2	3
36	12170	248.6	11.2	153.0	-8.8	NHHL	3	2
37	16334	187.5	45.8	152.7	-8.8	NHHL	3	3
38	39869	158.5	61.2	151.6	-8.8	NHHL	1	2
39	38366	227.6	16.0	145.7	-8.6	NHHL	3	3
40	59647	129.0	72.0	145.6	-8.6	NHHL	1	3
41	37965	88.7	56.0	144.7	-8.6	LL or SH	3	2
42	53259	146.1	56.8	140.0	-8.4	NHHL	3	3
43	14966	81.7	50.5	132.1	-8.2	LL or SH	2	3
44	57051	69.6	57.6	127.2	-8.0	LL or SH	2	2
45	37277	149.3	35.3	120.4	-7.8	NHHL	2	2

1140

Figure 1

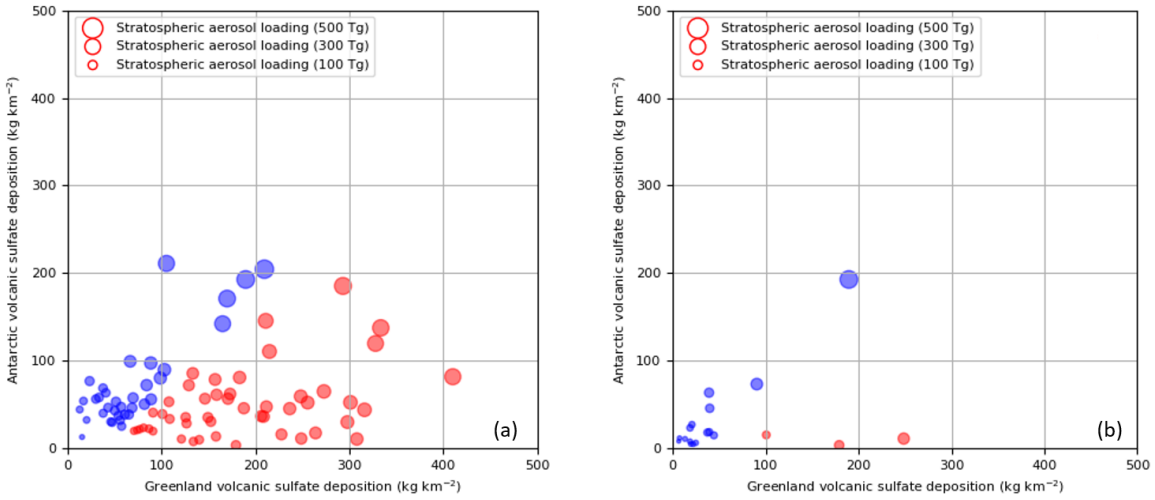

1145

1150

Figure 2

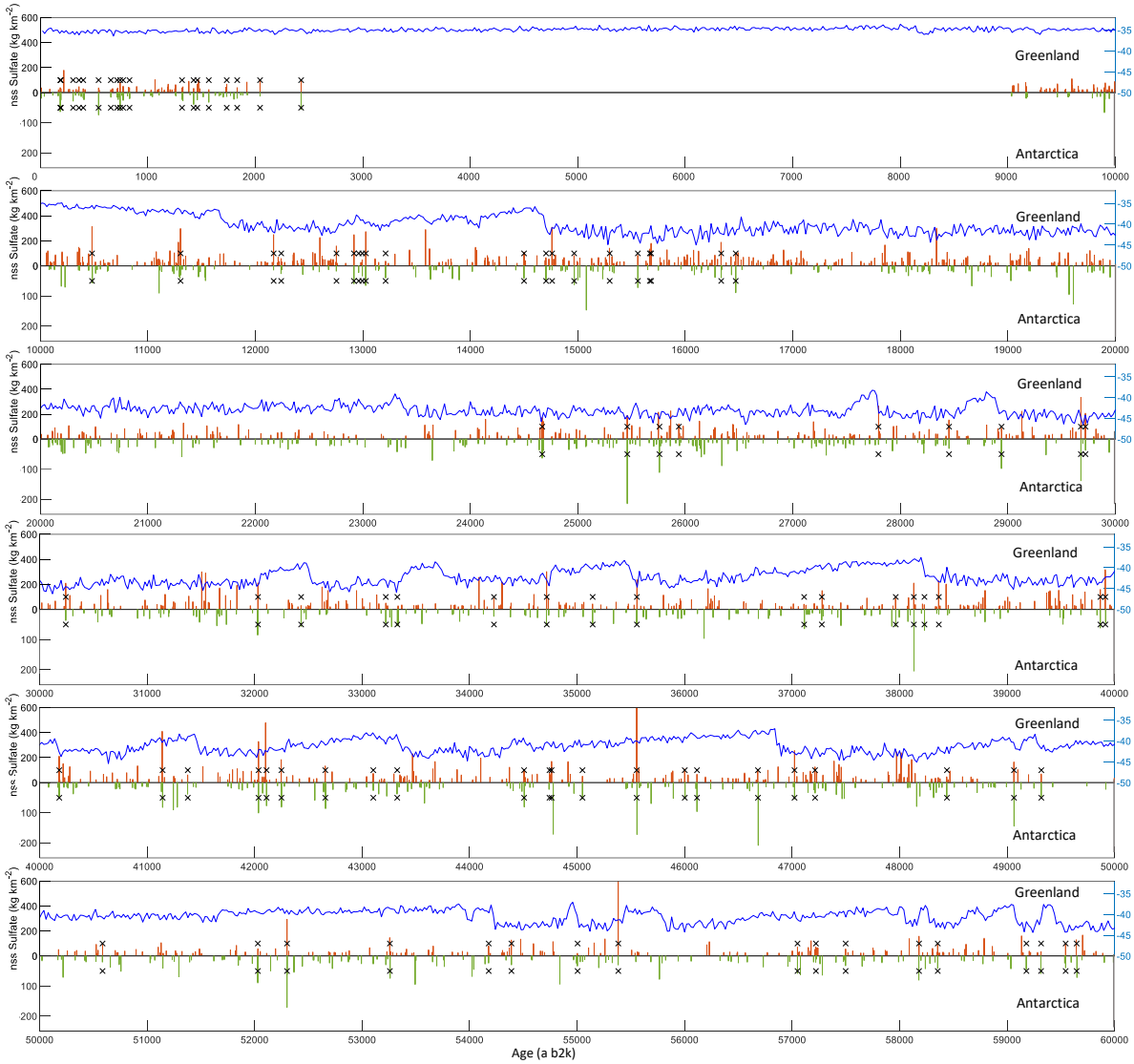
nss Sulfate (kg km^{-2})
Greenland
Antarctica
Age (a b2k)

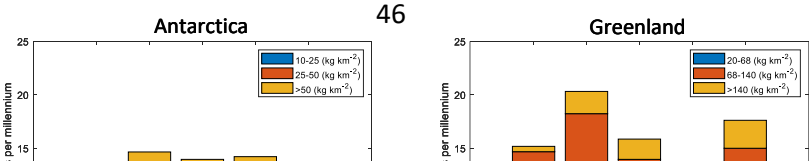
Antarctica
Greenland
10-25 (kg km^{-2})
25-50 (kg km^{-2})
>50 (kg km^{-2})
20-68 (kg km^{-2})
68-140 (kg km^{-2})
>140 (kg km^{-2})

Figure 3

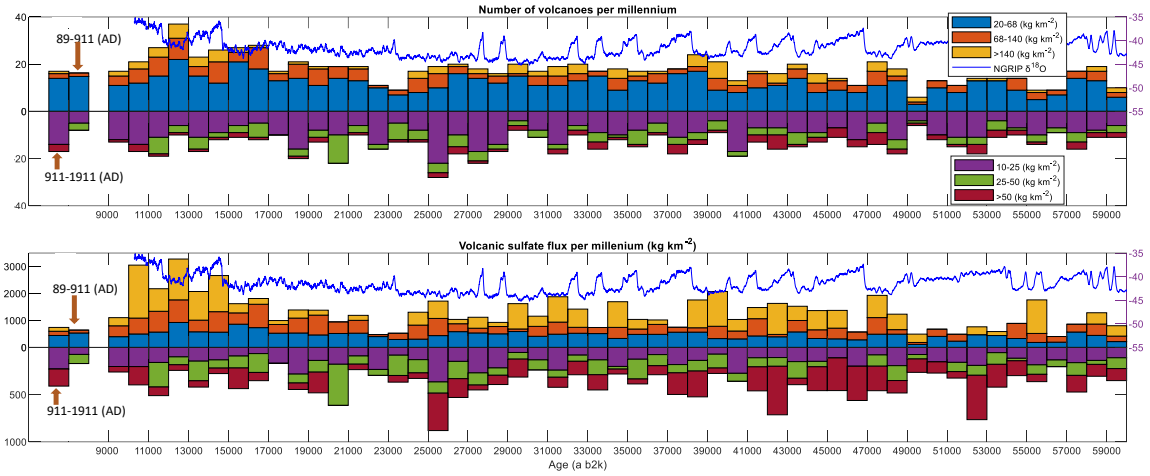

Figure 4

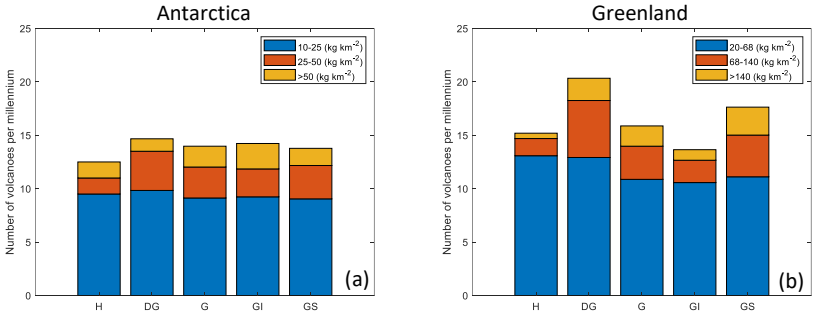

H = Holocene period (2-0 ka b2k)
DG = Deglacial period (21-9 ka b2k)
G = Glacial period (60-21 ka b2k)
GI = Glacial interstadials (60-21 ka b2k)
GS = Glacial stadials (60-21 ka b2k)

Figure 5

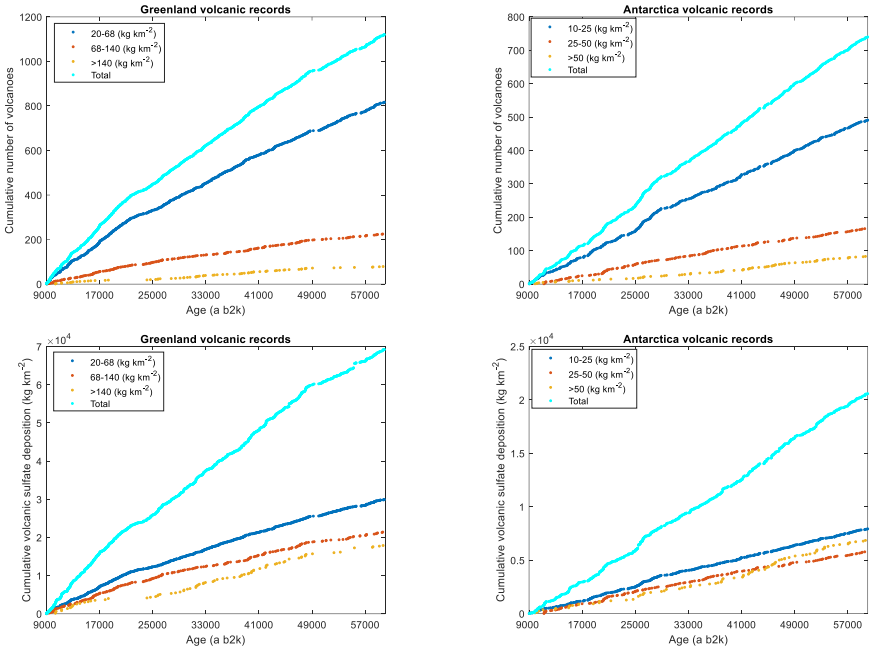
Greenland volcanic records
Cumulative number of volcanoes
Age (a b2k)
20-68 (kg km-2)
68-140 (kg km-2)
>140 (kg km-2)
Total
Antarctica volcanic records
10-25 (kg km-2)
25-50 (kg km-2)
>50 (kg km-2)
Total
Cumulative volcanic sulfate deposition (kg km-2)

Figure 6

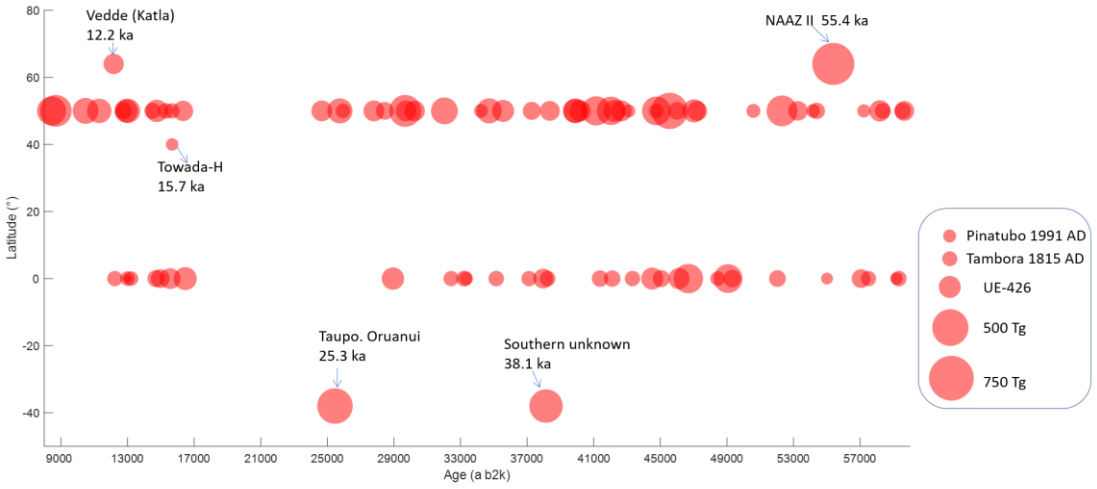
Vedde (Katla)
12.2 ka
NAAZ II 55.4 ka
Towada-H
15.7 ka
Taupo. Oruanui
25.3 ka
Southern unknown
38.1 ka
Latitude (°)
Age (a b2k)
Pinatubo 1991 AD
Tambora 1815 AD
UE-426
500 Tg
750 Tg